APPENDIX D

Underwater Sound Modelling of Seismic Survey and Development Activities Off-shore Newfoundland, Equinor's Bay du Nord Development Project (Zykov 2018)

Underwater Sound Modelling of Seismic Survey and Development Activities Off-shore Newfoundland

Equinor's Bay Du Nord Development Project

Submitted to:
David Robins
Wood PLC
Contract: 4600023752

Author:
Mikhail M. Zykov

15 July 2020

P001421-001
Document 01664
Version 2.1

JASCO Applied Sciences (Canada) Ltd
Suite 202, 32 Troop Ave.
Dartmouth, NS B3B 1Z1 Canada
Tel: +1-902-405-3336
Fax: +1-902-405-3337
www.jasco.com

Suggested citation:

Zykov, M.M. 2018. *Underwater Sound Modelling of Seismic Survey and Development Activities Off-shore Newfoundland: Equinor's Bay Du Nord Development Project*. Document 01664, Version 2.1. Technical report by JASCO Applied Sciences for Wood PLC

Disclaimer:

The results presented herein are relevant within the specific context described in this report. They could be misinterpreted if not considered in the light of all the information contained in this report. Accordingly, if information from this report is used in documents released to the public or to regulatory bodies, such documents must clearly cite the original report, which shall be made readily available to the recipients in integral and unedited form.

Contents

Figures

Tables

1. Introduction

JASCO Applied Sciences (JASCO) undertook a modelling study for Equinor Canada Ltd. (Equinor) to predict underwater sound levels associated with developing and operating the Bay Du Nord Project off-shore Newfoundland (Figure 1).

The Project development and operation would require various activities to be performed (seismic and geohazard surveys, drilling, etc.) that introduce acoustic noise into the water, which could potentially disturb marine mammals. At the time of this modelling study, the exact list of activities, locations, or the equipment had not been finalized. JASCO, in conjunction with Wood PLC, identified the activities that have the greatest impact in term of noise, the most likely locations for the acoustic sources, and specific equipment models that are commonly used for such activities.

The following operations/sources were modelled:

- A seismic survey,
- A geohazard survey using a sub-bottom profiler and a multi-beam sonar, and
- Vessels (drillship and floating production, storage, and offloading facility).

The goal of the modelling study was to estimate the root-mean-square (rms) pressure level, referred to as sound pressure level (SPL). The modelling also calculated the sound exposure level (SEL) field for a 24 h period (for vessels) or a section of a survey track (for seismic and geohazard surveys). As requested by Wood PLC, the SEL field was assessed against the impact thresholds outlined in the National Marine Fisheries Service's document *2018 Revision to: Technical Guidance for Assessing the Effects of Anthropogenic Sound on Marine Mammal Hearing (Version 2.0): Underwater Thresholds for Onset of Permanent and Temporary Threshold Shifts* (NMFS 2018). Peak SPL field was also calculated for the impulsive sources (a seismic survey source and geohazard survey sources).

The acoustic characteristics of the airgun array used for the seismic survey was modelled with JASCO's Airgun Array Source Model (Section 2.1), which accounts for individual airgun volumes and the array geometry. The source levels of the vessels were estimated based on the field measurements of a similar vessel. The source level directivity function of the sub-bottom profiler (SBP) and multi-beam sonar (MBES) were calculated using transducer beam theory.

The transmission loss was modelled with JASCO's Marine Operations Noise Model (Section 2.2) in the frequency range from 10 to 25,000 Hz. Sound propagation modelling was conducted to the ranges up to 150 km from a source.

The acoustic field modelling was performed at two locations (Site S1 and S2) within the Project Development Area (including one within the Core Development Area) for the airgun array source (Figure 1) and at one location within the Core Development Area for the vessels and geohazard survey sources. At each location, the modelling was performed for two sound speed profiles in the water column (February and August) to consider the annual variation of the sound propagation conditions (Section 3.1).

For greater accuracy, the SPL and peak SPL fields for the airgun array source were estimated based on the full waveform modelling that provides time-domain representations of the pressure waves generated in the water.

The 24 h SEL fields for the vessels were calculated using stationary source assumption and for the seismic and geohazard sources assuming a static animal, but a moving sound source (the "Safe Distance" methodology as indicated in NMFS (2018)).

The SEL and peak SPL fields were assessed against the threshold levels for the onset of Permanent Threshold Shift (PTS) and Temporary Threshold Shift (TTS) relevant to each marine mammal group using respective auditory weighting functions as per NMFS (2018).

Section 2 details the methodology for predicting the source levels (Section 2.1) and modelling the sound propagation (Section 2.2). Section 3 describes the input parameters to the propagation modelling: the assumed environmental parameters (Section 3.1), modelling receiver geometry (Section 3.2), and

specifications and derived source levels of the acoustic sources (Section 3.3). Also Section 3 provides the list of modelled scenarios (Section 3.4) and approach for estimating the marine mammal exposure in case of a moving source (Section 3.5). Section 4 presents results of the modelling study as sound field contour maps and tables of distances to sound level thresholds for the SPL fields, and as schematics of threshold contours and tables of Safe Distances to the specific thresholds for sound exposure levels. Additional modelling results as tables of the maximum levels at specific ranges from the seismic source are provided in Appendix A. Appendix B explains the signal metrics used to represent underwater acoustic fields, and Appendix C the impact criteria considered.

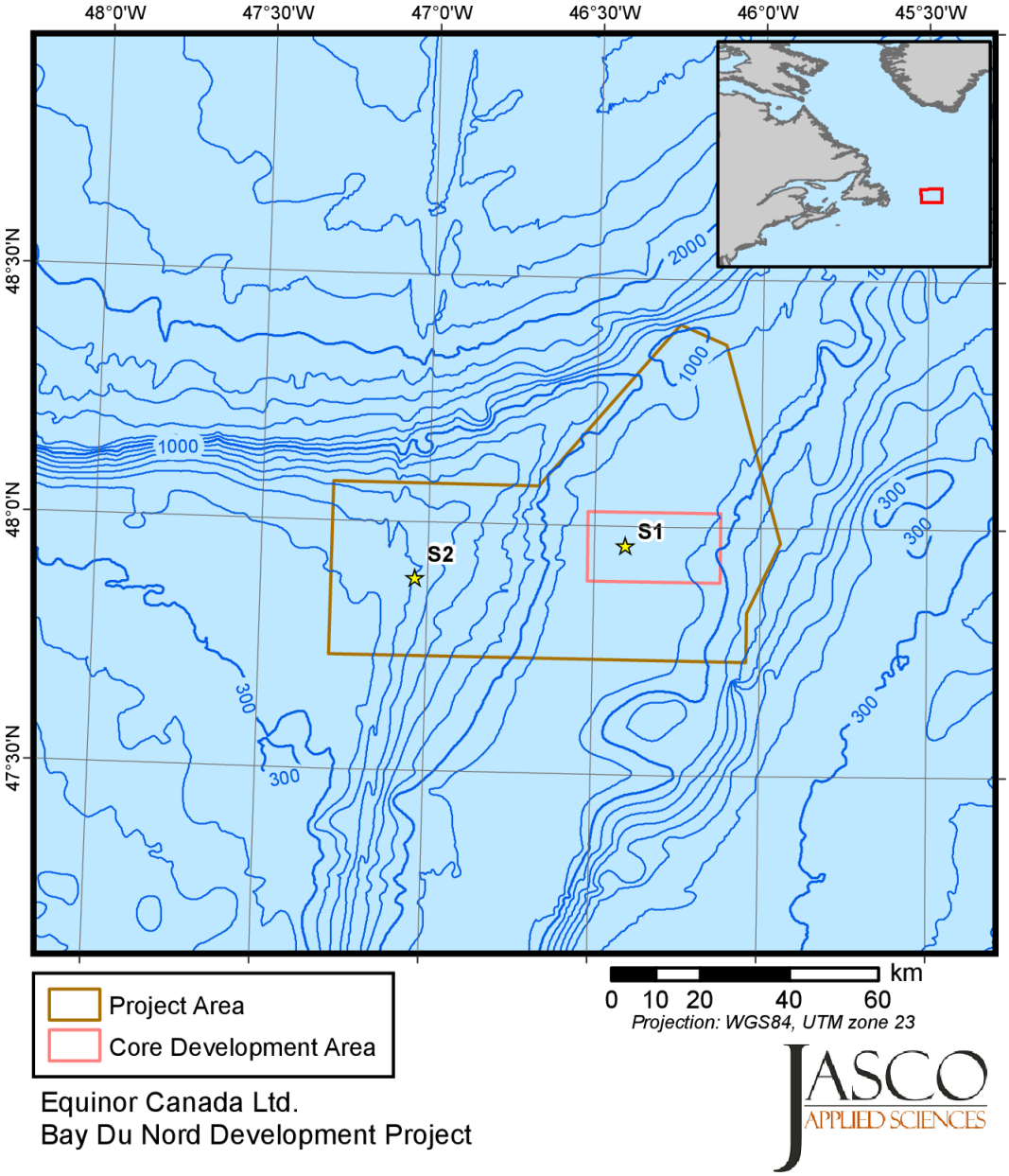

Figure 1. Project area overview and modelled locations (yellow stars) for the Bay Du Nord Development Project. Blue contours indicate water depth in meters.

2. Methods

The prediction of the underwater acoustic fields was completed in two steps:

1. Modelling of the source level function, and
2. Modelling of the pressure wave propagation around the source.

JASCO employed various acoustic source function models and acoustic wave propagation models. The models were selected based on the source characteristics and the required output. Models incorporated parameters specific to the sources and the environments.

2.1. Acoustic Source Models

2.1.1. Seismic airgun array

The modelled acoustic sources were conventional airguns. The source levels and directivity of the airgun array were predicted with AASM. This model is based on the physics of the oscillation and radiation of airgun bubbles as described by Ziolkowski (1970). The model solves the set of parallel differential equations that govern bubble oscillations. AASM also accounts for non-linear pressure interactions between airguns, port throttling, bubble damping, and Generated Injection (GI) airgun behaviour, as discussed by Dragoset (1984), Laws et al. (1990), and Landro (1992). AASM includes four empirical parameters that are tuned so that the model output matches observed airgun behaviour. The model parameters were fit to a large library of empirical airgun data using a "simulated annealing" global optimization algorithm (Černý 1985). These airgun data consist of measured signatures of Bolt 600/B airguns that range in volume from 5 to 185 in^3; the provided sampling rate of the time series was 50 kHz (Racca and Scrimger 1986).

AASM produces a set of notional signatures for each airgun element based on:

- Array spatial layout
- Volume, tow depth, and operating pressure of each airgun
- Interactions between airguns in the array

Notional signatures are the pressure waveforms of the individual airguns at a standard reference distance of 1 m; they account for the interactions between the air bubbles created by adjacent airguns in the array. The signatures are summed with the appropriate phase delays to obtain the far-field source signature of the entire array in the horizontal plane. This far-field[1] array signature is filtered into 1/3-octave passbands to compute the source levels of the array as a function of frequency band and azimuthal angle in the horizontal plane (at the source depth). It can then be treated as a point source in the far-field.

A seismic array consists of many sources and the point-source assumption is invalid in the near field where the array elements add incoherently. The maximum extent of the near field of an array (R_{nf}) is:

$$R_{nf} < \frac{l^2}{4\lambda} \tag{1}$$

where λ is the sound wavelength and l is the longest dimension of the array (Lurton 2002, §5.2.4). For example, an airgun array length of $l \approx 16$ m yields a near-field range of 85 m at 2 kHz and 17 m at

[1] The far-field is the zone where, to an observer, sound originating from a spatially-distributed source appears to radiate from a single point.
The distance to the acoustic far field increases with frequency.

100 Hz. Beyond R_{nf}, it is assumed that an array radiates like a directional point source and is treated as such for propagation modelling.

The AASM accurately predicts the source level of each complete array as a point source for the purpose of acoustic propagation modelling in the far-field; however, predicted source levels for 0 to peak SPL and SEL metrics could be higher than the possible maximum levels during the array operation even within the array. AASM accounts for the effects of source depth on bubble interactions, the surface-reflected signal (i.e., surface ghost) is excluded from the far-field source signatures. The propagation models account for surface reflections, a property of the medium rather than the source.

The separations between individual elements of the array in the horizontal plain create directionality in overall acoustic emissions. Generally, this directivity is prominent mainly at frequencies in the mid-range of several tens to several hundreds of hertz; at lower frequencies, where acoustic wavelengths are much larger than the inter-airgun separation distances, directivity is small. At higher frequencies the pattern of lobes becomes too finely spaced to be resolved and the effective directivity is less.

The AASM model can predict the far-field airgun array signature in the frequency range from 10 to 25,000 Hz.

2.1.2. High-frequency engineering sources

Mid- and high-frequency underwater acoustic sources for geophysical measurements create an oscillatory overpressure through rapid vibration of a surface, using either electromagnetic forces or the piezoelectric effect of some materials. A vibratory source based on the piezoelectric effect is commonly referred to as a transducer, and it might be capable of receiving as well as emitting signals. Transducers are usually designed to produce an acoustic wave of a specific frequency, often in a highly directive beam. The directional capability increases with increasing operating frequency. The main parameter characterizing the directivity is the beamwidth, defined as the angle subtended by diametrically opposite “half power” (−3 dB) points of the main lobe. For different transducers, the beamwidth can vary from 180° (almost omnidirectional) to only a few degrees.

Transducers are usually built with either circular or rectangular active surfaces. For circular transducers the beamwidth in the horizontal plane (assuming a downward pointing main beam) is equal in all directions. Rectangular transducers produce more complex beam patterns with variable beamwidth in the horizontal plane; two beamwidth values are usually specified for orthogonal axes.

The acoustic radiation pattern, or beam pattern, of a transducer is the relative measure of the acoustic power as a function of spatial angle. Directionality is generally measured in decibels relative to the maximum radiation level along the central axis, perpendicular to the transducer surface. The pattern is defined largely by the operating frequency, size, and shape of the transducer.

Beam patterns generally consist of a main lobe, extending along the central axis of the transducer, and multiple secondary lobes separated by nulls. The width of the main lobe depends on the size of the active surface relative to the sound wavelength in the medium, with larger transducers producing narrower beams. Figure 2 presents a 3-D visualization of a generic beam pattern of a circular transducer.

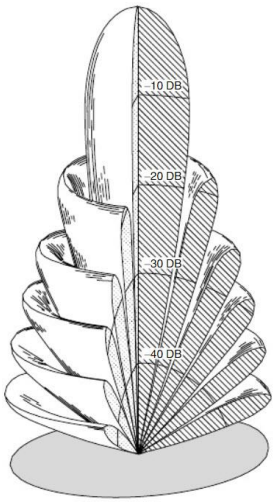

Figure 2. Typical 3-D beam pattern of a circular transducer (Massa 2003).

The beamwidth, a key characteristic of transducers, is generally defined as the total angular range where the sound pressure level of the main beam is within 3 dB of the on-axis peak power (Massa 2003).

2.1.2.1. Beam Pattern of a Circular Transducer

The beam of an ideal circular transducer is symmetric about the main axis; the radiated level depends only on the depression angle. In this study, beam directivities were calculated from the standard formula for the beam pattern of a circular transducer (Kinsler et al. 1950, ITC 1993). The directivity function of a conical beam relative to the on-axis pressure amplitude is:

$$R(\phi) = \frac{2\,J_1(\pi D_\lambda \sin\phi)}{\pi\, D_\lambda \sin\phi}, \qquad D_\lambda = {}^{60}/_{\theta_{\mathrm{bw}}} \tag{2}$$

where $J_1(\phi)$ is the first-order Bessel function, D_λ is the transducer dimension in wavelengths of sound in the medium, θ_{bw} is the beamwidth in degrees, and ϕ is the beam angle from the transducer axis. The beam pattern of a circular transducer can be calculated from the transducer's specified beamwidth or from the diameter of the active surface and the operating frequency.

Although some acoustic energy is emitted at the back of the transducer, the theory accounts for the beam power in only the front half-space (ϕ < 90°) and assumes no energy directed into the back half-space. The relative power at these rearward angles is significantly lower, generally by more than 30 dB, and consequently the emission in the back half-space can be estimated by applying a simple decay rate, in decibels per angular degree, which gives a beam power at ϕ = 90° of 30 dB less than that at ϕ = 0°. This is a conservative estimate of the beam power in the back half-space.

2.1.2.2. Beam Pattern of a Rectangular Transducer

Rectangular transducer beam directivities were calculated from the standard formula for the beam pattern of a rectangular acoustic array (Kinsler et al. 1950, ITC 1993). This expression is the product of the toroidal beam patterns of two line arrays where the directional characteristics in the along- and across-track directions are computed from the respective beamwidths. The directivity function of a toroidal beam relative to the on-axis pressure amplitude is:

$$R(\phi) = \frac{\sin(\pi L_\lambda \sin\phi)}{\pi L_\lambda \sin\phi}, \qquad L_\lambda = {}^{50}/_{\theta_{\mathrm{bw}}} \tag{3}$$

where L_λ is the transducer dimension in wavelengths, θ_{bw} is the beamwidth in degrees, and ϕ is the angle from the transducer axis. Here again, the beam pattern of a transducer can be calculated using either the specified beamwidth in each plane or the dimensions of the active surface and the operating frequency of the transducer.

2.1.3. Vessels

Underwater sound that radiates from vessels is produced mainly by propeller and thruster cavitation, with a smaller fraction of noise produced by sound transmitted through the hull, such as by engines, gearing, and other mechanical systems. Sound levels tend to be the highest when thrusters are used to position the vessel and when the vessel is transiting at high speeds. A vessel's sound signature depends on the vessel's size, power output, propulsion system (e.g., conventional propellers vs. Voith Schneider propulsion), and the design characteristics of the given system (e.g., blade shape and size). A vessel produces broadband acoustic energy with most of the energy emitted below a few kilohertz.

Common approach for defining the source levels for vessels is to use field measurements completed on a similar vessel of the same type ("surrogate" vessel) involved in a similar activity. The measured spectrum is taken unchanged while the broad band source level is adjusted to account for any difference in the total propulsion power between the reference vessel and the vessel of interest. The adjusted broad band source level is calculated as:

$$SL = SL_{ref} + 10\log\left(\frac{P}{P_{ref}}\right), \tag{4}$$

where SL_{ref} is the broad band source level of the surrogate vessel, P and P_{ref} are the total propulsion power of the vessel of interest and the surrogate vessel, respectively.

2.2. Sound Propagation Modelling

2.2.1. Transmission loss

The propagation of sound through the environment can be modelled by predicting the acoustic transmission loss—a measure, in decibels, of the decrease in sound level between a source and a receiver some distance away. Geometric spreading of acoustic waves is the predominant way by which transmission loss occurs. Transmission loss also happens when the sound is absorbed and scattered by the seawater, and absorbed scattered, and reflected at the water surface and within the seabed. Transmission loss depends on the acoustic properties of the ocean and seabed; its value changes with frequency.

If the acoustic source level (SL), expressed in dB re 1 µPa²·s, and transmission loss (TL), in units of dB, at a given frequency are known, then the received level (RL) at a receiver location can be calculated in dB re 1 µPa @ 1 m by:

$$\mathrm{RL} = \mathrm{SL} - \mathrm{TL} \tag{5}$$

The transmission loss based acoustic propagation models are suitable for estimation of the SEL filed, as they cannot predict the change of other characteristics of the pulse such as length and amplitude, which are essential for calculating the SPL field.

JASCO employs MONM for the transmission loss based modelling. MONM predicts underwater sound propagation (i.e., transmission loss) at frequencies of 10 Hz to 25 kHz. Combined with a source level prediction, this model can compute the received per-pulse SEL for directional impulsive sources at a specified depth. MONM employs two underlaying subroutines: MONM-RAM is used for propagating acoustic waves at low frequencies (10 to 1600 Hz) and MONM-BELLHOP is used for high frequencies (above 2000 Hz and to hundreds of kHz).

MONM-RAM computes acoustic propagation via a wide-angle parabolic equation solution to the acoustic wave equation (Collins 1993) based on a version of the U.S. Naval Research Laboratory's Range-dependent Acoustic Model (RAM), which has been modified to account for an elastic seabed (Zhang and Tindle 1995). The parabolic equation method has been extensively benchmarked and is widely employed in the underwater acoustics community (Collins et al. 1996). MONM-RAM accounts for the additional reflection loss at the seabed due to partial conversion of incident compressional waves to shear waves at the seabed and sub-bottom interfaces, and it includes wave attenuations in all layers. MONM-RAM incorporates the following site-specific environmental properties: a modelled area bathymetric grid, underwater sound speed as a function of depth, and a geoacoustic profile based on the overall stratified composition of the seafloor. MONM-RAM accounts for the azimuthal (horizontal) variability of the sound level of the emitted pulse of the source.

MONM-BELLHOP computes sound propagation via the BELLHOP Gaussian beam acoustic ray-trace model (Porter and Liu 1994). This version of MONM accounts for sound attenuation due to energy absorption through ion relaxation and viscosity of water in addition to acoustic attenuation due to reflection at the medium boundaries and internal layers (Fisher and Simmons 1977). The former type of sound attenuation is significant for frequencies higher than 5 kHz and cannot be neglected without noticeably affecting the model results. MONM-BELLHOP accounts for the variability of the sound level of the emitted pulse with both azimuth and depression angles according to the 3-D beam pattern of the source.

MONM's predictions have been validated against experimental data from several underwater acoustic measurement programs conducted by JASCO (Hannay and Racca 2005, Aerts et al. 2008, Funk et al. 2008, Ireland et al. 2009, O'Neill et al. 2010, Warner et al. 2010, Racca et al. 2012a, Racca et al. 2012b, Martin et al. 2015).

2.2.2. Full waveform

For impulsive sounds, time-domain representations of the pressure waves generated in the water are required to calculate SPL and peak pressure level. The synthetic pressure waveforms can be computed using FWRAM, which is a time-domain acoustic model based on the same wide-angle parabolic equation (PE) algorithm as MONM. FWRAM computes synthetic pressure waveforms versus range and depth (Figure 3) for range-varying marine acoustic environments, and it takes the same environmental inputs as MONM (bathymetry, water sound speed profile, and seabed geoacoustic profile). Unlike MONM, FWRAM computes pressure waveforms via Fourier synthesis of the modelled acoustic transfer function in closely spaced frequency bands. FWRAM employs the array starter method to accurately model sound propagation from a spatially distributed source (MacGillivray and Chapman 2012).

The FWRAM modelling method is significantly more computationaly extensive compared to the transmission loss based modelling. Therefore, it is performed within a narower frequency band (usually 10-512/1024 Hz) and smaller number of modelling profiles. Since the majority of the acoustic energy emmited by a seismic source is below 500 Hz and SPL and peak SPL metric is calculated on an unweighted field, the narower modelled frequency band does not affect the accuracy of the modelling.

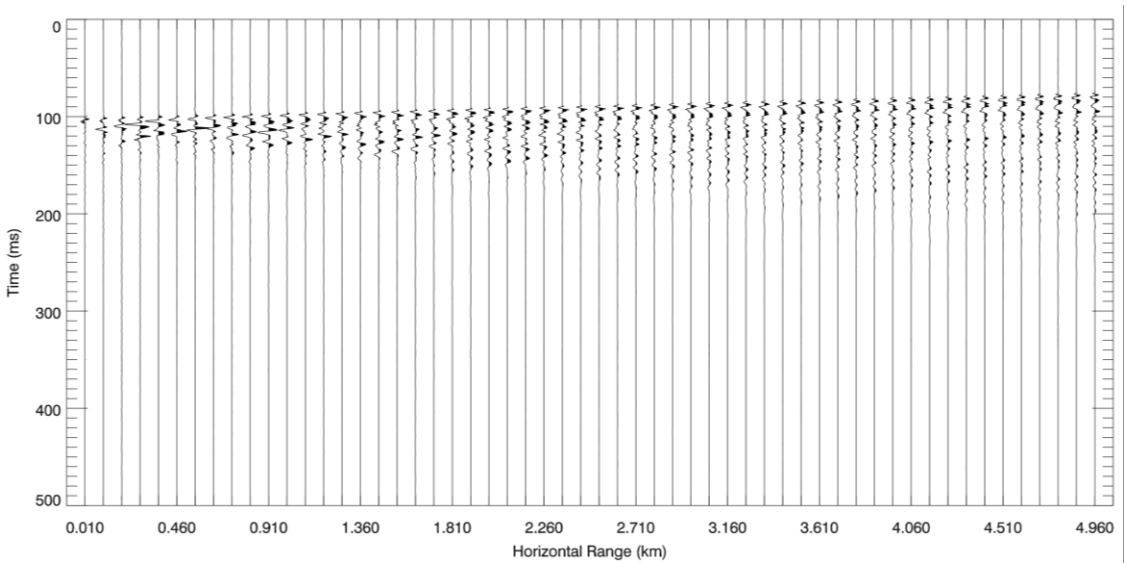

Figure 3. Example of synthetic pressure waveforms computed by FWRAM.

2.2.3. N×2-D volume approximation and maximum-over-depth sampling

While the core propagation models within MONM are limited to 2-D acoustic propagation only, MONM computes acoustic fields in three dimensions by modelling transmission loss within two-dimensional (2-D) vertical planes aligned along radials covering a 360° swath from the source, an approach commonly referred to as *N*×2-D. These vertical radial planes are separated by an angular step size of $\Delta\theta$, yielding $N = 360°/\Delta\theta$ number of planes (Figure 4).

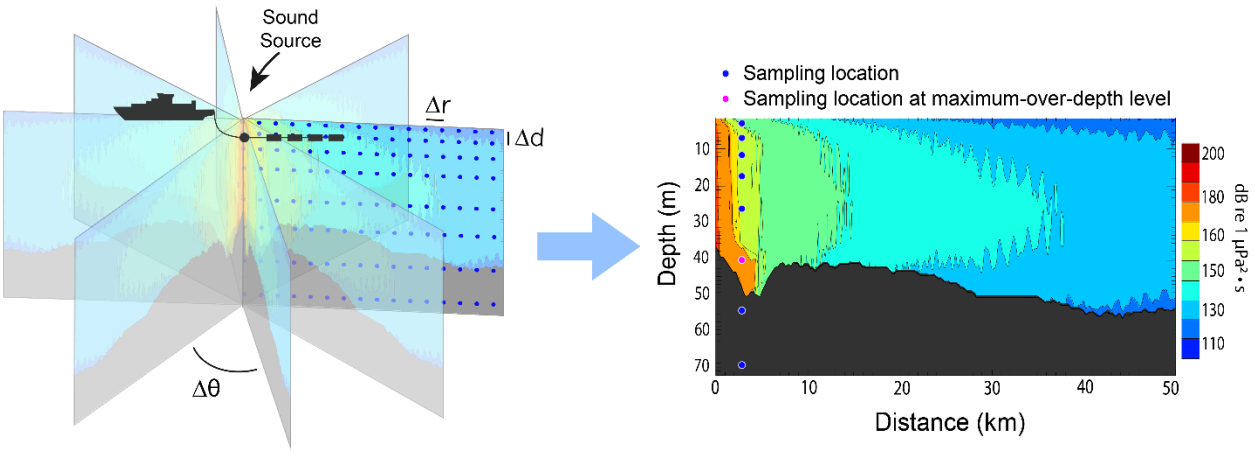

Figure 4. The *N*×2-D and maximum-over-depth modelling approach used by MONM.

The received per-pulse SEL sound field within each vertical radial plane is sampled at various ranges from the source, generally with a fixed radial step size (Δr in Figure 4). At each sampling range along the surface, the sound field is sampled at various depths (Δd in Figure 4), with the step size between samples increasing with depth below the surface. The step sizes are chosen to provide increased coverage near the depth of the source and at depths of interest in terms of the sound speed profile. For areas with deep water, sampling is not performed at depths beyond those reachable by marine mammals. The received per-pulse SEL at a surface sampling location is taken as the maximum value that occurs over all samples within the water column, i.e., the maximum-over-depth received per-pulse SEL. These maximum-over-depth per-pulse SELs are further used to calculate the ranges to specific thresholds and create acoustic field maps.

2.3. Sound Exposure Levels from a Moving Source

Sound exposure levels from a moving source were modelled using the "Safe Distance" methodology in NMFS (2018), which is recommended as a "less sophisticated model" for mobile sources and static receivers (Figure 5). The Safe Distance approach accounts for the source level, the source's speed, and duty cycle. It assumes static receivers and that the acoustic wave's propagation is limited to spherical spreading (NMFS 2018). The Safe Distance is defined as the distance from the source beyond which a threshold for the metric is not exceeded NMFS (2018). With a mobile source, "the distance from the source" is substituted with the distance from the source track.

The calculations of the Safe Distance for this report were performed with the following improvements to the NMFS (2018) methodology, aimed to increase their accuracy:

- Source directivity is accounted for.
- A sophisticated sound propagation model is used to calculate the per-pulse sound fields, instead of a very basic "spherical spreading" approach.
- The actual source activation pattern, which is the position of the source when the acoustic pulse was delivered, is incorporated into the calculations.

To calculate the Safe Distance (R_{SD}), the SEL field is calculated for the duration over which the source operates over a section of the survey track. The SEL for the track field is calculated by summing the modelled marine mammal frequency weighted (see Appendix C.2.1) M-weighted per-pulse SEL of source impulses originating from the locations defined by the source activation pattern. The length of the source track section is selected to be sufficiently large such, that including additional pulses before and after the selected section does not change the Safe Distance at the Closest Point of Approach (CPA). The Safe

Distance is determined at the CPA by finding the maximum distance from the source track at which the specific threshold is exceeded.

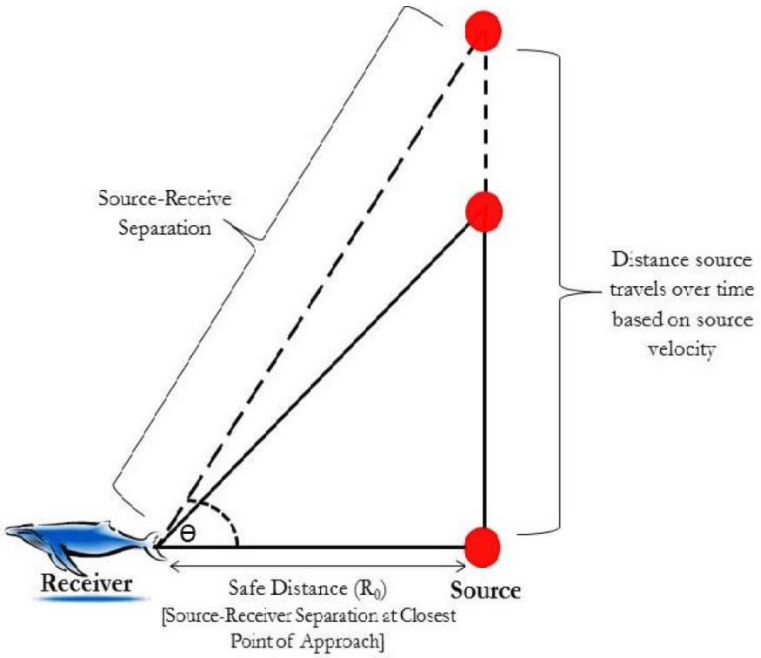

Figure 5. Schematics from NMFS (2018) explaining the Safe Distance approach for mobile sources and static receivers (Figure D5 from NMFS 2018).

3. Model Parameters

3.1. Environmental Parameters

The water depths within the Core Development Area range from 1000 to 1200 m and within the Project Area from 350 to 1200 m. One modelling site was selected within the Core Development Area and second site was selected in the shallow part of the Project Area (Table 1). Figure 1 shows the site locations. The acoustic field from the seismic source was modelled at both sites, while vessels and geohazard survey sources were modelled at Site S1 only.

Table 1. Proposed modelling locations and their parameters.

Site	Geographic coordinates	UTM coordinates (Zone 23 North)	Water depth at source (m)
S1	47° 57.7' N 46° 24.4' W	395000E 5313000N	1180
S2	47° 53.4' N 47° 02.0' W	348000E 5306000N	500

3.1.1. Bathymetry

Water depths throughout the modelled area were extracted from the SRTM15+ global bathymetry grid, a 15 arc-second grid (~300 × 450 m at the studied latitude) rendered for the entire globe (Smith and Sandwell 1997, Becker et al. 2009). Bathymetry data were extracted from the global grid and re-gridded onto a Universal Transverse Mercator (UTM) Zone 23 coordinate projection with a regular grid spacing of 300 × 300 m.

3.1.2. Geoacoustics

The geoacoustic properties of surficial layers depend on the sediment type. As the porosity decreases, the compressional sound speed, sediment bulk density, and compressional attenuation increase. For each modelled location, MONM assumes a single geoacoustic profile of the seafloor for the entire modelled area.

MONM used these geoacoustic properties of the sediments:

- Bulk density (g/cm^3),
- Compressional-wave (or P-wave) speed (m/s),
- P-wave attenuation in decibels per wavelength (dB/λ),
- Shear-wave (or S-wave) speed (m/s), and
- S-wave attenuation in decibels per wavelength (dB/λ).

The geoacoustic parameters were calculated using a sediment grain-shearing model (Buckingham 2005), which computes the acoustic properties of the sediments from porosity and grain-size measurements. The grain size and the porosity variation with depth were estimated based on the expected bottom sediment type. Table 2 presents the full set of geoacoustic parameters used for the acoustic propagation modelling. Same set of parameters was used at both sites.

Table 2. Geoacoustic properties of the sub-bottom sediments as a function of depth, in meters below the seafloor (mbsf). Within each depth range, each parameter varies linearly within the stated range.

Depth (mbsf)	Material	Density (g/cm^3)	P-wave speed (m/s)	P-wave attenuation (dB/λ)	S-wave speed (m/s)	S-wave attenuation (dB/λ)
0–5	Silt mixed with sand and clay	1.5–1.7	1525–1585	0.25–0.40	200	3.65
5–50		1.7–2.0	1585–1775	0.40–0.75		
50–500		2.0–2.1	1775–2100	0.75–1.4		
> 500		2.1	2100	1.4		

3.1.3. Sound speed profiles

The sound speed profiles were derived using temperature and salinity profiles from the U.S. Naval Oceanographic Office's *Generalized Digital Environmental Model V 3.0* (GDEM; Teague et al. 1990, Carnes 2009). GDEM provides an ocean climatology of temperature and salinity for the world's oceans on a latitude-longitude grid with 0.25° resolution, with a temporal resolution of one month, based on global historical observations from the U.S. Navy's Master Oceanographic Observational Data Set (MOODS). The climatology profiles include 78 fixed depth points to a maximum depth of 6800 m (where the ocean is that deep), including 55 standard depths between 0 and 2000 m. The GDEM temperature-salinity profiles were converted to sound speed profiles according to Coppens (1981).

Figure 6 presents sound speed profiles at Site S1 for the months selected for modelling (February and August). The same sound speed profile was used to model at both sites (S1 and S2).

The sound speed profile for February features a strong surface channel and provides the most favourable sound propagation conditions with the least attenuation. In August, strong downward refracting propagation conditions exist in the top 50 m of the water column with the presence of deep sound channel.

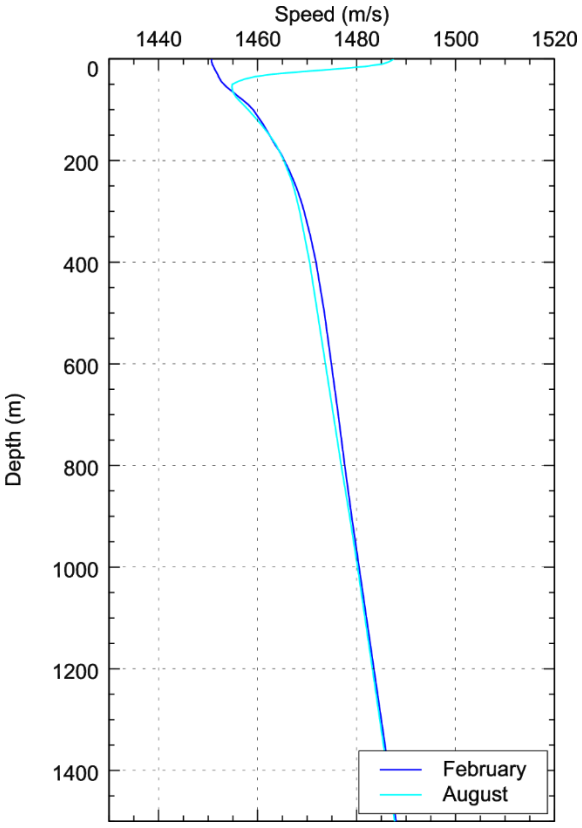

Figure 6. Sound speed profile in the water column for February and August (GDEM profile location 48.0°N 47.0°W), derived using monthly temperature and salinity data obtained from *GDEM V 3.0* (Teague et al. 1990, Carnes 2009).

3.2. Geometry and Modelled Volumes

The modelling geometry for each source was selected individually based on the parameters of the source and required output (Table 3).

Table 3. Modelling geometry for the individual sources.

Source	Metric	N-profiles (azimuthal step)	Horizontal resolution (m)	Max. distance (km)
Airgun array	SEL	72 (5°)	20	100
Airgun array	SPL and peak SPL	5 (selected)	Variable, 10 to 500	150
Vessels	SEL and SPL	72 (5°)	20	50
Sub-bottom profiler	SEL and SPL	72 (5°)	5	5
Multi-beam echosounder	SEL and SPL	180 (2°)	5	5

At each surface sampling location, the sound field was sampled at the following depths:

- 2 m
- Every 5 m from 5 to 25 m
- Every 25 m from 50 to 100 m
- Every 50 m from 150 to 500 m
- Every 100 m from 500 to 1000 m
- Every 200 m from 1200 to 2000 m

In addition to the fixed sampling depths, the sound field was sampled at the bottom.

The model used a tow direction of 270° for all sites.

3.3. Acoustic Source Parameters and Modelled Source Levels

3.3.1. Seismic survey source - 5085 in³ airgun array

At the time of the modelling project execution, the exact seismic source that would be used for the seismic survey was unknown. JASCO suggested to model WG 5085 in³ seismic array as a proxy source. This source has been modelled previously by JASCO for other seismic surveys proposed in the Canadian Atlantic waters.

The WG 5085 in³ array is ~18 × 15 m in size and consists of 24 elements aligned in 3 identical strings and is towed at a 10 m depth. The size of the individual elements of the array varies from 105 in³ to 290 in³. The firing pressure was modelled at 2000 psi. The array layout is shown in Figure 7 and detailed in Table 4.

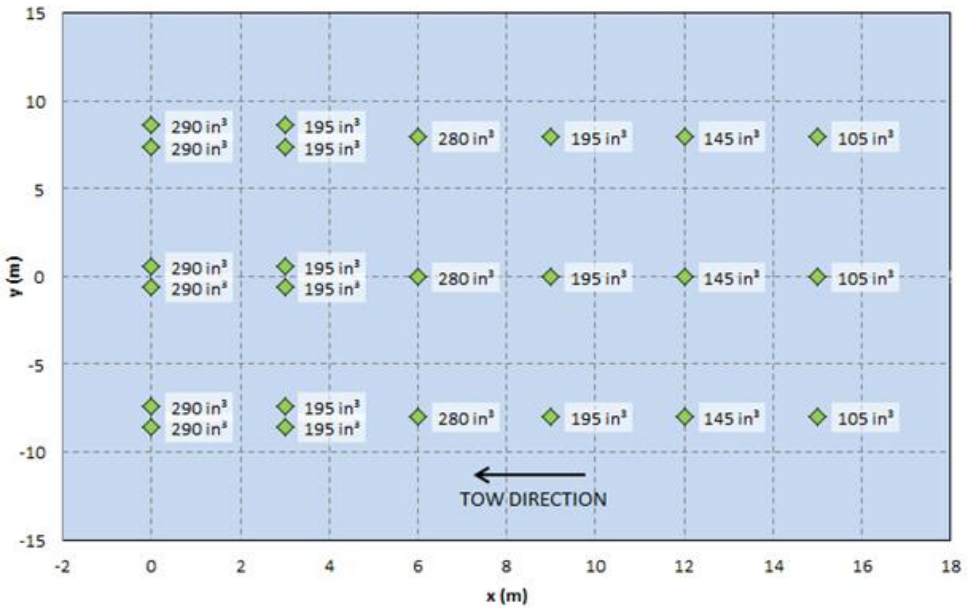

Figure 7. Layout of the active elements of the 5085 in³ array. Tow depth is 10 m. Labels indicate element volumes.

Table 4. Coordinates of the elements within the 5085 in³ array. Tow depth is 10 m. Each section of the table represents a subarray.

Gun	*x* (m)	*y* (m)	Volume (in³)	Gun	*x* (m)	*y* (m)	Volume (in³)	Gun	*x* (m)	*y* (m)	Volume (in³)
1	0	8.5	290	9	0	0.5	290	17	0	−7.5	290
2	0	7.5	290	10	0	−0.5	290	18	0	−8.5	290
3	3	8.4	195	11	3	0.4	195	19	3	−7.6	195
4	3	7.6	195	12	3	−0.4	195	20	3	−8.4	195
5	6	8	280	13	6	0	280	21	6	−8	280
6	9	8	195	14	9	0	195	22	9	−8	195
7	12	8	145	15	12	0	145	23	12	−8	145
8	15	8	105	16	15	0	105	24	15	−8	105

The pressure signatures of the individual airguns and the composite 1/3-octave-band source levels of the arrays, as functions of azimuthal angle (in the horizontal plane), were modelled with AASM (see Section 2.1.1).

The broadside (perpendicular to the tow direction) and endfire (parallel to the tow direction) horizontal overpressure signatures and corresponding power spectrum levels for the 5085 in³ array towed at a depth of 10 m are shown in Figure 8. The signatures (Figure 8a) consist of a strong primary peak, related to the initial firing of the airguns, followed by a series of pulses associated with the bubble oscillations. Most energy is produced at frequencies below 750 Hz (Figure 8b). Frequency-dependent peaks and nulls in the spectrum result from interference among airguns in the array and reflect the volumes and relative locations of the airguns.

Horizontal 1/3-octave-band source levels are shown as a function of band centre frequency and azimuth (Figure 9). Directivity in the sound field was most noticeable at mid-frequencies from 60 to 400 Hz. Broadside and endfire 1/3-octave-band unweighted source levels and M-weighted source levels for NMFS (2018) M-weighting function are presented in Figure 10. The maximum band source level after mid- and high-frequency cetacean M-weighting applied occurs at 8000 Hz and at 25,000 Hz drops more than 15 dB below maximum. This indicates that the selection of the modelling frequency range up to 25,000 Hz is correct for the fields that are analysed using M-weighting functions.

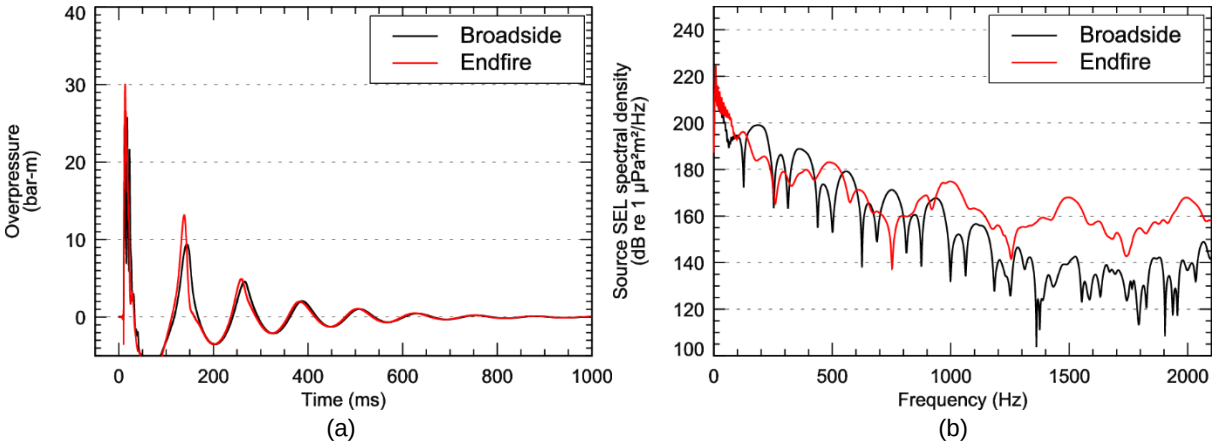

Figure 8. Predicted (a) overpressure signature and (b) power spectrum in the broadside and endfire (horizontal) directions for the 5085 in³ array.

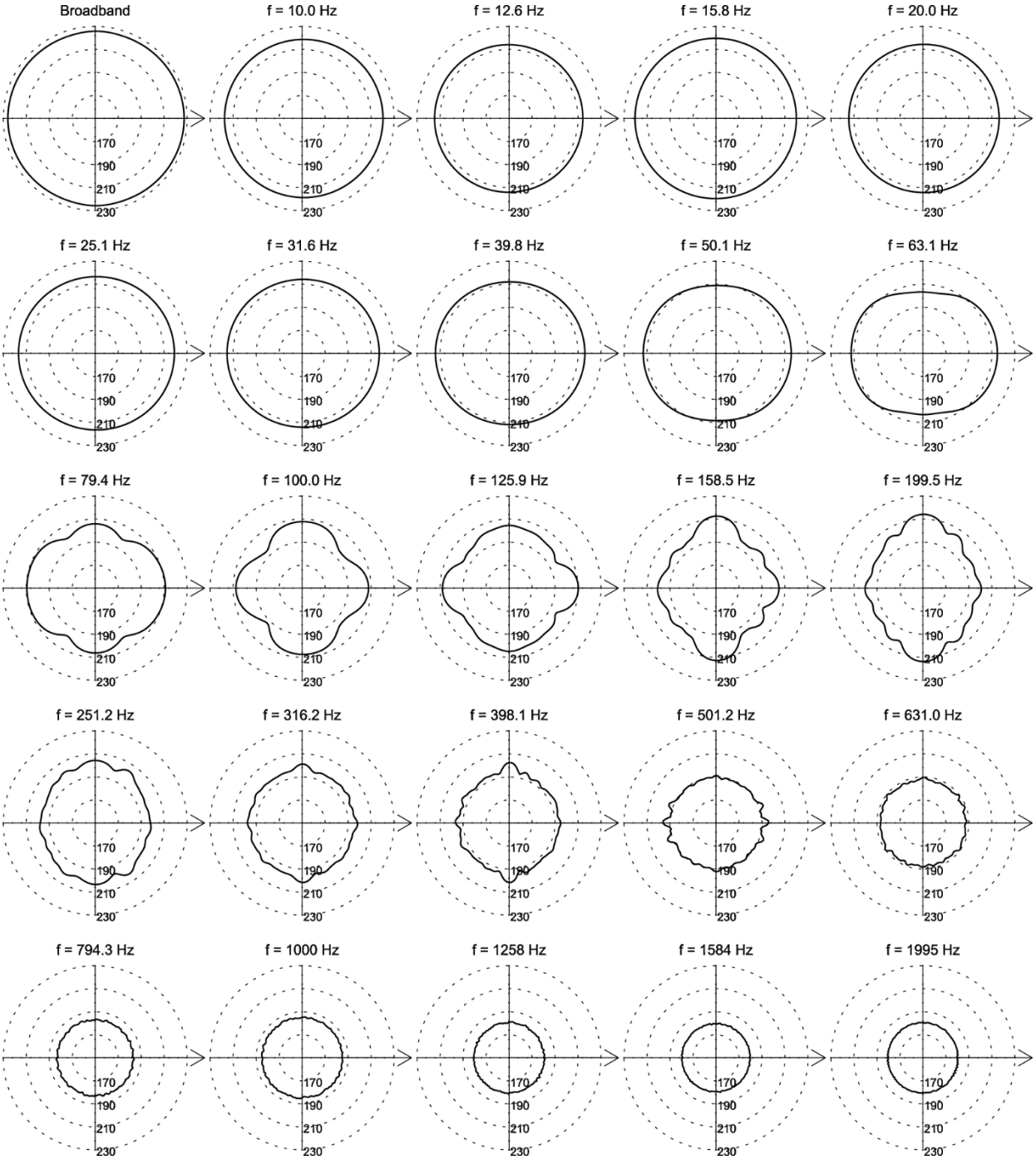

Figure 9. Directionality of the predicted horizontal source levels for the 5085 in^3 array. Source levels (in dB re 1 µPa^2·s) are shown as a function of azimuth for the centre frequencies of the 1/3-octave-bands modelled; frequencies are indicated above each plot. Tow direction is to the right. Tow depth is 10 m.

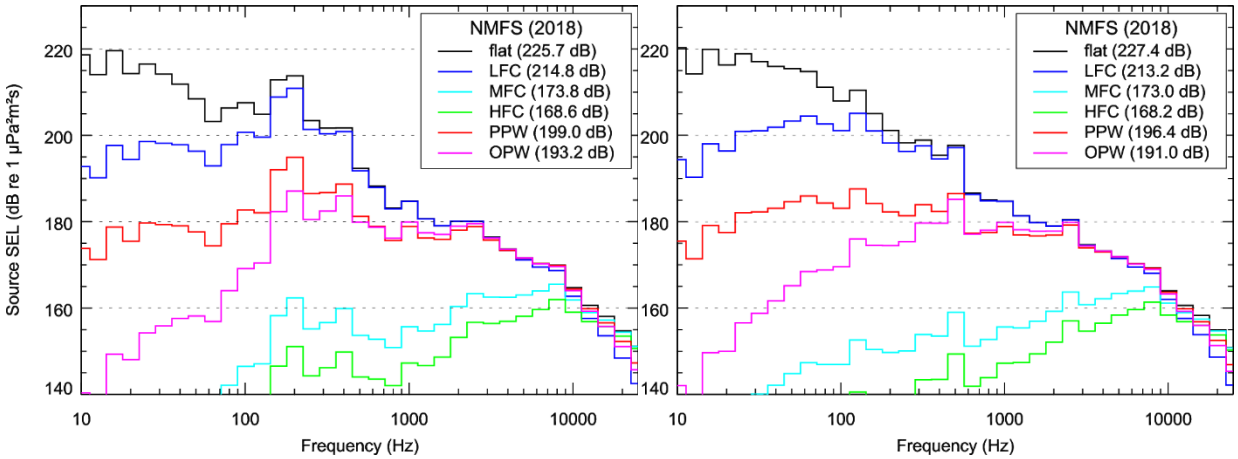

Figure 10. (Left) Broadside and (right) endfire 1/3-octave-band unweighted (flat) source levels in the horizontal plane for the 5085 in³ seismic array and M-weighted source levels using NMFS (2018) weighting functions for the five marine mammal groups (see Appendix C.2.1). The values in brackets following the abbreviated group show broadband source levels after M-weighting was applied. LFC=Low-frequency cetaceans. MFC=Mid-frequency cetaceans. HFC=High-frequency cetaceans. PPW=Phocid pinnipeds in water. OPW=Otariid pinnipeds in water.

3.3.2. Geohazard survey sources

Sub-bottom profiler (SBP) and multi-beam echosounder (MBES) were identified as potential sources for the geohazard surveys.

3.3.2.1. Sub-bottom profiler

The EdgeTech 3300 was selected as a proxy source to represent the sub-bottom profiler source for the Project. The profiler transducer produces a full-spectrum chirp signal in the frequency band from 2 to 16 kHz. The central lobe of the circular beam pattern is 20° wide. The maximum engagement rate is 15 Hz with a pulse duration of 20 ms. The source level of the transducer is 212 dB re 1 µPa peak SPL, 209 dB re 1 µPa SPL, and 192 dB re 1 µPa²·s SEL.

The beam pattern calculations were based on the standard formula for the beam pattern of a circular transducer (Equation 2), with a decay rate in the back half space of 0.25 dB per degree from the horizontal plane. Figure 11 presents vertical slice of the calculated beam patterns for the EdgeTech 3300 using a 20° beamwidth. The operational frequency range of the transducer spans over eight 1/3-octave-bands. It was assumed that the source level spectrum is flat with 183 dB re 1 µPa²·s SEL per band.

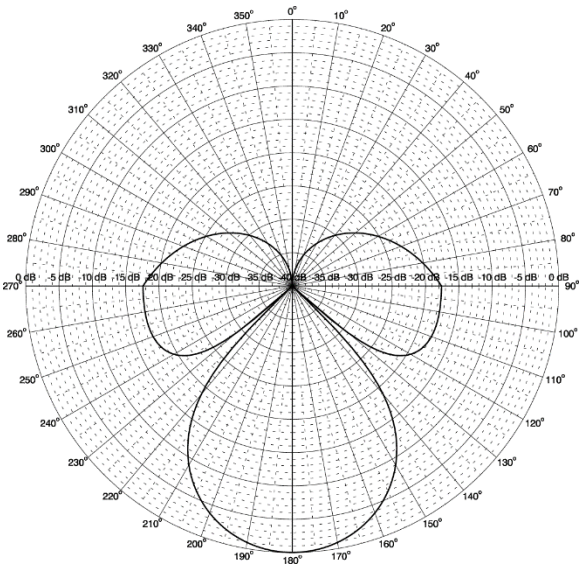

Figure 11. Calculated beam pattern vertical slice for the EdgeTech 3300, using a 20° beamwidth.

3.3.2.2. Multi-beam echosounder

The Simrad EM2000 was selected as a proxy source to represent the multi-beam echosounder source for the Project. The echosounder transducer produces a narrow band signal at 200 kHz. The beamwidth is 120° in the cross-track direction and 17° in the along-track direction. The maximum ping rate is 10 Hz with a pulse duration of 0.2 ms. The source level of the transducer is 218 dB re 1 µPa peak SPL, 215 dB re 1 µPa SPL, and 178 dB re 1 µPa²·s SEL.

The beam pattern calculations were based on the standard formula for the beam pattern of a rectangular transducer (Equation 3), with a decay rate in the back half space of 0.25 dB per degree from the horizontal plane. Figure 12 presents vertical slice of the calculated beam patterns for the Simrad EM2000.

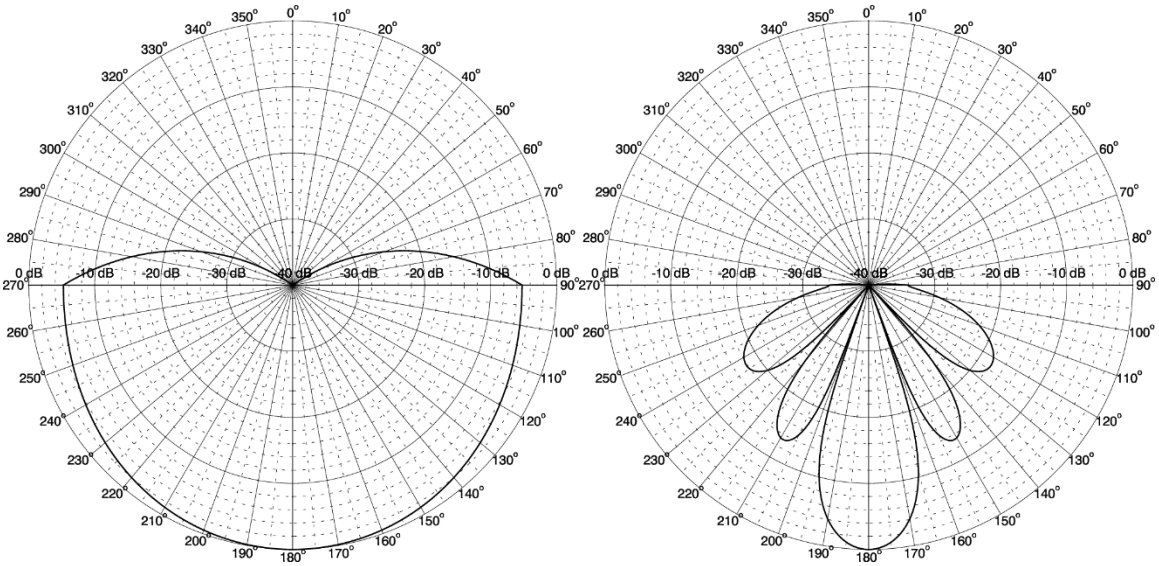

Figure 12. Calculated beam pattern vertical slice for the Simrad EM2000 multibeam echosounder across-track (left) and along-track (right) directions.

3.3.3. Vessels

Multiple types of vessels are expected to be active in the area during Project development. A floating production, storage, and offloading (FPSO) facility and a drillship were identified as the largest vessel and also the vessels that will introduce the most acoustic noise into the environment. When this modelling study was completed, the exact FPSO vessel had not yet been selected. *Stena Carron* was identified as the drillship of choice.

JASCO has previously modelled acoustic fields from an FPSO facility (see McPherson et al. 2016). The modelled FPSO facility was a dynamically positioned (DP) vessel approximately 280 m long and 50 m wide with an 18 m draft. When in DP mode, it operates on two stern thrusters, each rated at 3.0 MW.The source levels of the FPSO facility were derived from the field measurements of *Fu Lai* vessel by adjusting for the difference of the propulsion power using Equation 4 assuming 50% power output of the DP thrusters. The results of the FPSO facility source level from McPherson et al. (2016) were taken as reported. The broad band source level of the FPSO facility was 183.7 dB re 1 µPa.

Stena Carron is a 228 m long and 42 m wide, harsh environment, DP class 3 drillship with total DP thrust output power of 33 MW. The draft of *Stena Carron* during drilling operations is 12 m. The source levels for *Stena Carron* were derived from the source levels for the FPSO by adjusting for the difference in the propulsion power using Equation 4 assuming 50% power output of the DP thrusters. The broad band source level of *Stena Carron* was 187.6 dB re 1 µPa.

Figure 13 shows the 1/3-octave-band source levels for the FPSO facility and *Stena Carron* used as input for the acoustic field modelling.

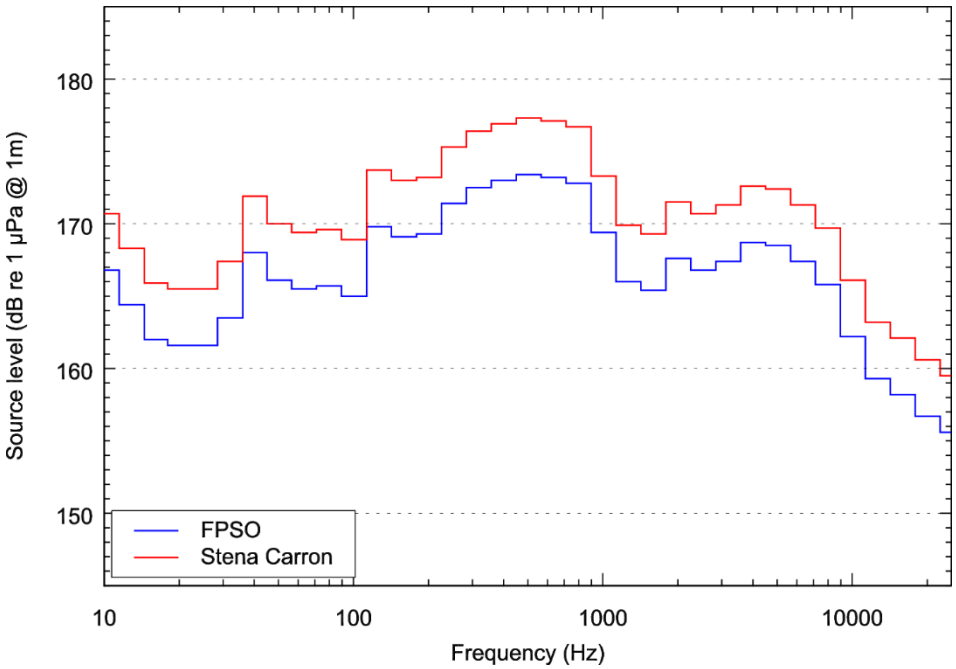

Figure 13. Source levels in 1/3-octave-bands for the FPSO facility and *Stena Carron*.

3.4. Modelled Scenarios

The seismic survey source was modelled at two sites, and at each site two propagation conditions were considered. Vessel activities and geohazard surveys are supposed to occur only within the Core Development Area and were therefore modelled only at Site S1. The sound fields for vessels were modelled considering two propagation conditions. There were two individual vessel sources (*Stena Carron* and FPSO facility) and one multi-vessel source. The geohazard survey sources were modelled only for February propagation conditions. There were two geohazard survey sources (SBP and MBES). The summary of the modelled scenarios is provided in Table 5.

Table 5. Summary of modelled scenarios.

Source type	Number of sources	Site	Propagation condition	Number of scenarios
Seismic survey source	1	S1 and S2	February and August	4
Geohazard survey sources	2	S1	February	2
Vessels	3	S1	February and August	6

3.5. Sound Exposure Level Modelling from Seismic Source

The impact criteria based on the SEL field require estimating the SEL over a time period. For the vessel scenarios, it was assumed that the sound source is stationary, and the source level does not vary with time.

The seismic and geohazard survey scenarios apply the Safe Distance (see Section 2.3) approach that considers a moving source and static animal. The SEL for a section of a survey track was calculated using actual source engagement pattern and assuming that the per-pulse SEL field does not change much as the source progresses along the track, i.e., the same per-pulse SEL field was used to represent the exposure from each of the shots.

For the purpose of modelling of the Safe Distance from a seismic survey profile, a seismic survey was considered with a single source. The source engagement was set to be every 37.5 m along the track.

The geohazard survey sources were set be engaged every 2 m along the track.

The Safe Distances were determined based on the sound exposure field from a 20 km long section of the source track (10 km on each side of the CPA). The length of the modelled track was selected to be long enough to provide stable safe distance values at the CPA (i.e., the safe distance values do not increase with the extension of the modelled track).

4. Acoustic Field Modelling Results

4.1. Seismic Survey Source

The 5058 in³ airgun array was modelled at both sites (Site S1 and S2). At each site, the modelling was performed using two sound speed profiles, representing the propagation conditions typical for February and August. In total, the seismic source was modelled for four scenarios.

In addition to the acoustic modelling results presented in this section, tables of the signal levels at specific ranges from the source are provided in Appendix A.

4.1.1. SPL and Peak SPL

The SPL and peak SPL for the seismic source were estimated based on the full waveform modelling (see Section 2.2.2). The modelling was performed along five transects at each site: four to test the propagation conditions with different water depth profiles, plus one transect at 180° to test the broadside azimuth of the source (Figure 14). The SPL and peak SPL were calculated directly from the synthetic pressure waveforms.

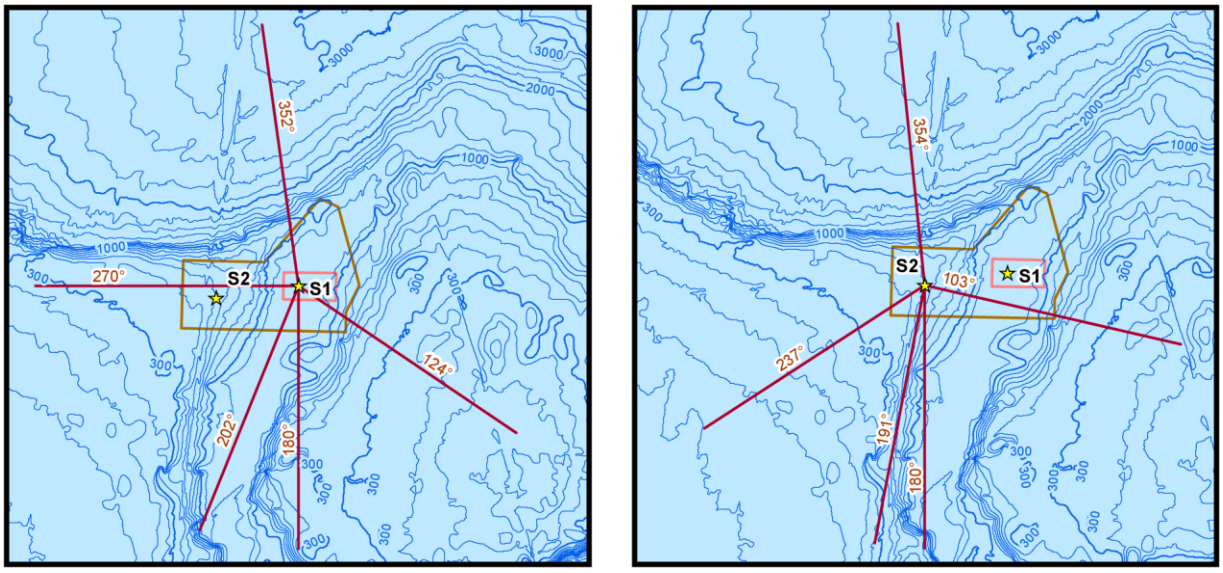

Figure 14. Profiles used for full waveform modelling. The degree values indicate the azimuth of each profile. The length of each profile is 150 km.

The predicted distances to specific levels were computed from the maximum-over-depth sound fields. Two distances, relative to the source, are reported for each SPL threshold (Table 6): (1) R_{max}, the maximum range at which the given sound level was encountered in the modelled maximum-over-depth sound field, and (2) $R_{95\%}$, the maximum range at which the given sound level was encountered after excluding 5% of the farthest such points. Maximum range to the PTS- and TTS-onset thresholds defined for the peak SPL field are presented in Table 7.

Examples of the vertical distribution of the peak SPL and SPL fields for the 5085 in³ seismic array at Site S1 for the 124° transect are provided on Figures 15 and 16 (for the February and August propagation conditions, respectively). The full set of vertical distribution plots for peak SPL, SPL, and SEL along all modelled profiles, and all scenarios were provided as an appendix external to this report.

Table 6. 5058 in³ airgun array: Maximum (R_{max}, m) and 95% ($R_{95\%}$, m) horizontal distances from the 5085 in³ source to modelled maximum-over-depth SPL thresholds.

SPL (dB re 1 µPa)	Site S1				Site S2			
	February		August		February		August	
	R_{max}	$R_{95\%}$	R_{max}	$R_{95\%}$	R_{max}	$R_{95\%}$	R_{max}	$R_{95\%}$
210	<40	<40	<40	<40	<40	<40	<40	<40
200	50	50	50	50	60	50	60	50
190	179	159	179	159	199	159	199	159
180	596	517	577	527	886	727	876	717
170	2560	2240	2560	2230	2750	2240	2760	2270
160	20100	15400	10700	8540	20100	16000	9310	7520
150	121000	93500	79500	25600	137000	92600	43600	23900
140	>150000	>150000	144000	96600	>150000	>150000	144000	123000
130			>150000	>150000			>150000	>150000

Table 7. 5058 in³ airgun array: Maximum horizontal distances in metres from the source to PTS- and TTS-onset thresholds defined for the peak SPL field (NMFS 2018).

Marine mammal group	PTS-onset					TTS-onset				
	peak SPL (dB re 1 µPa)	Site S1		Site S2		peak SPL (dB re 1 µPa)	Site S1		Site S2	
		Feb	Aug	Feb	Aug		Feb	Aug	Feb	Aug
Low-frequency cetaceans	219	<40	<40	<40	<40	213	50	50	50	50
Mid-frequency cetaceans	230	<40	<40	<40	<40	224	<40	<40	<40	<40
High-frequency cetaceans	202	179	189	179	189	196	368	368	358	368
Phocid pinnipeds (underwater)	218	<40	<40	<40	<40	212	60	60	60	60
Otariid pinnipeds (underwater)	232	<40	<40	<40	<40	226	<40	<40	<40	<40

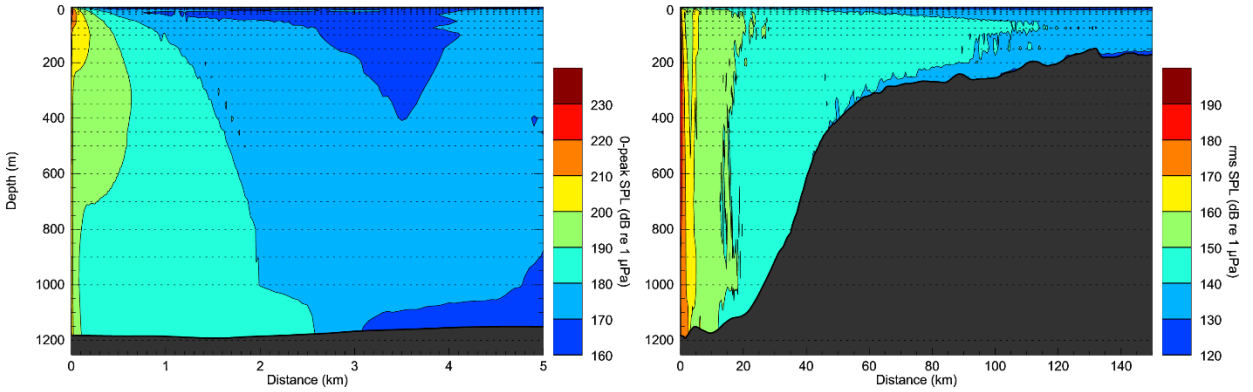

Figure 15. 5058 in³ airgun array: Modelled vertical distribution of the peak SPL (left) and SPL (right) fields at Site S1, 124° transect, February propagation conditions.

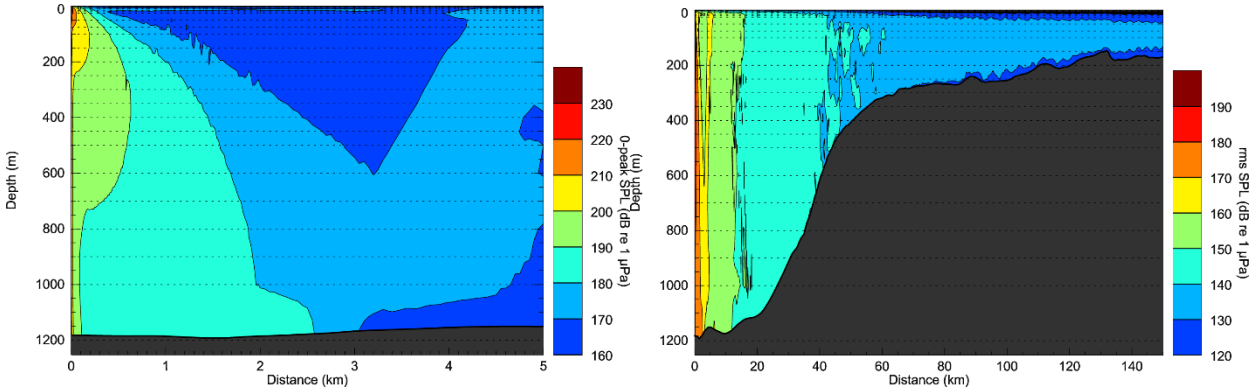

Figure 16. 5058 in³ airgun array Vertical slice of the modelled peak SPL (left) and SPL (right) fields at Site S1, 124° transect, August propagation conditions.

4.1.2. Sound Exposure Levels

The calculations of the SEL for a track used modelled per-pulse SEL fields that were modelled at each of the sites for two propagation conditions. An example of the per-pulse SEL field at Site S1 for February and August propagation conditions are shown on Figure 17.

Sound exposure levels were calculated with the methodology for the Safe Distance estimation for mobile sources and static receivers described in NMFS (2018), but were enhanced to account for the source directivity and propagation environment properties (see Section 2.3).

The Safe Distance (R_{SD}) was estimated for each marine mammal group using M-weighting functions and specific TTS- and PTS-onset thresholds defined in NMFS (2018) for impulsive source. The calculations were performed for a seismic survey source engagement pattern (see Section 3.3) at each of the two sites for February and August propagation conditions using modelled per-pulse fields at the respective sites. The results are presented as a table of Safe Distances (Table 8). For all marine mammal groups and types of thresholds, the modelling provided definitive values, with the exception of the range to the TTS for low-frequency cetaceans. The Safe Distance value did not achieve stability for modelled 20 km long profile, as it increased as the modelled profile length increased. It would take ~2.5 hours for a seismic vessel moving with standard survey speed to pass the 20 km stretch of the seismic profile. Because it was unreasonable to assume that a whale would be stationary for such a long time, the modelling was not performed for a longer stretch. Since the exact Safety Distance was not calculated, the value for the range to TTS for low-frequency cetaceans was reported as being larger than the modelled grid limit, i.e., greater than 5000 m.

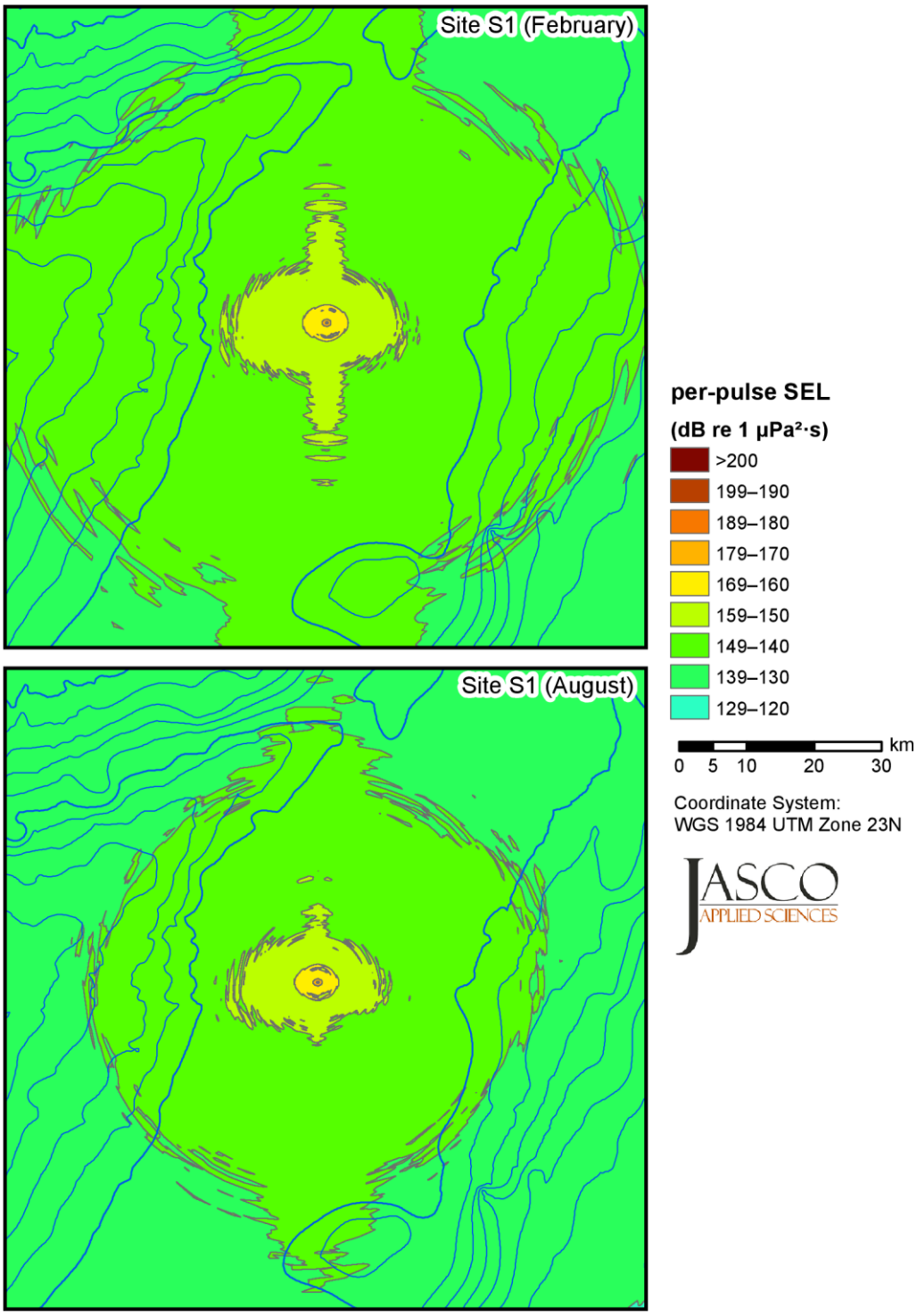

Figure 17. 5058 in³ airgun array; Modelled non-weighted per-pulse SEL field at Site S1 for (top) February and (bottom) August propagation conditions.

Table 8. 5058 in³ airgun array; Safe distances in metres from a seismic survey track to PTS- and TTS-onset thresholds (NMFS 2018) based on the SEL field for a track.

Marine mammal group	PTS-onset					TTS-onset				
	SEL (dB re 1 µPa²·s)	Site S1		Site S2		SEL (dB re 1 µPa²·s)	Site S1		Site S2	
		Feb	Aug	Feb	Aug		Feb	Aug	Feb	Aug
Low-frequency cetaceans	183	131	131	161	151	168	>5000	>5000	>5000	>5000
Mid-frequency cetaceans	185	<40	<40	<40	<40	170	<40	<40	<40	<40
High-frequency cetaceans	155	<40	<40	<40	<40	140	181	111	181	119
Phocid pinnipeds (underwater)	185	<40	<40	<40	<40	170	71	71	71	71
Otariid pinnipeds (underwater)	203	<40	<40	<40	<40	188	<40	<40	<40	<40

4.2. Geohazard Survey Sources

For the purpose of modelling the acoustic impact from geohazard surveys, the operation of sub-bottom profiler and multi-beam echosounder were modelled. Both devices were considered in a hull mounted option. EdgeTech 3300 was used as a proxy for the sub-bottom profiler, and Simrad EM2000 was used to represent multi-beam echosounder. The geohazard survey sources were modelled at Site S1 only, within the Core Development Area and propagation conditions for February (worst case scenario).

The modelling was performed for 72 and 180 transects for the sub-bottom profiler and multi-beam echosounder, respectively to 5 km from the source. The modelling frequency range was from 2.5 to 12.5 kHz for the sub-bottom profiler and single frequency at 200 kHz for the multi-beam echosounder.

4.2.1. SPL and Peak SPL

For the sub-bottom profiler and multi-beam echosounder, it was assumed that the pulse width does not change significantly during propagation, and SPL was estimated using transmission loss approach. The peak SPL was estimated using spherical spreading approach assuming 20·log(R) decay of the peak acoustic pressure with range.

The underwater sound fields predicted by the propagation models were sampled such that the received sound level at each point in the horizontal plane was taken to be the maximum value over all modelled depths for that point (Section 2.2.3). The resultant maximum-over-depth SPL fields are presented below in two formats: as tables of distances to sound levels and as contour maps showing the directivity and range to various sound levels.

The predicted distances to specific levels were computed from the maximum-over-depth sound fields. Two distances, relative to the source, are reported for each sound level: (1) R_{max}, the maximum range at which the given sound level was encountered in the modelled maximum-over-depth sound field, and (2) $R_{95\%}$, the maximum range at which the given sound level was encountered after excluding 5% of the farthest such points.

The distances to the sound level thresholds from 200 to 120 dB re 1 µPa SPL with 10 dB step both geohazard survey sources at Site S1 for February propagation conditions are presented in Table 9. The

contour maps of the estimated acoustic fields in SPL are presented in Figure 18. Maximum range to the PTS- and TTS-onset thresholds defined for the peak SPL field are presented in Table 10.

Vertical slices of the modelled SPL field for sub-bottom profiler and multi-beam echosounder are presented on Figures 19 and 20, respectively.

Table 9. Sub-bottom profiler and multi-beam echosounder: Maximum (R_{max}, m) and 95% ($R_{95\%}$, m) horizontal distances to modelled maximum-over-depth SPL thresholds. Site S1, February propagation conditions.

SPL (dB re 1 µPa)	MBES		SBP	
	R_{max}	$R_{95\%}$	R_{max}	$R_{95\%}$
200	<5	<5		
190	5	5		
180	20	20	<5	<5
170	65	60	7	7
160	150	135	30	30
150	275	240	99	96
140	430	368	279	269
130	715	567	623	586
120	900	783	3920	3830

Table 10. Sub-bottom profiler and multi-beam echosounder: Maximum horizontal distances in metres to PTS- and TTS-onset thresholds defined for the peak SPL field (NMFS 2018). Dash indicates that the peak SPL source levels of the device is below the threshold.

Marine mammal group	PTS-onset			TTS-onset		
	peak SPL (dB re 1 µPa)	MBES	SBP	peak SPL (dB re 1 µPa)	MBES	SBP
Low-frequency cetaceans	219	—	—	213	<5	—
Mid-frequency cetaceans	230	—	—	224	—	—
High-frequency cetaceans	202	40	10	196	158	40
Phocid pinnipeds (underwater)	218	<5	—	212	<5	<5
Otariid pinnipeds (underwater)	232	—	—	226	—	—

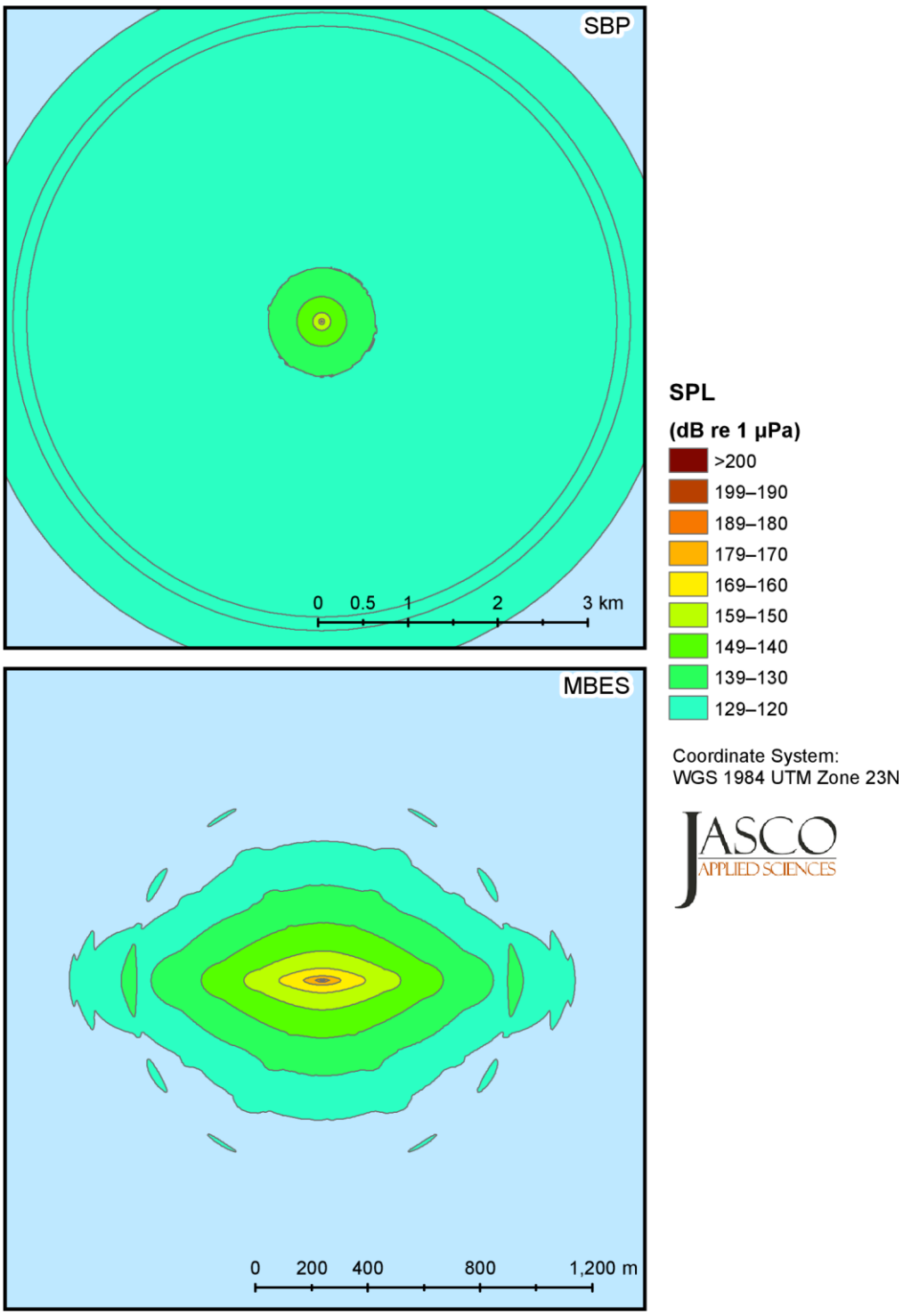

Figure 18. Sub-bottom profiler and multi-beam echosounder: Modelled SPL field at Site S1, February propagation conditions.

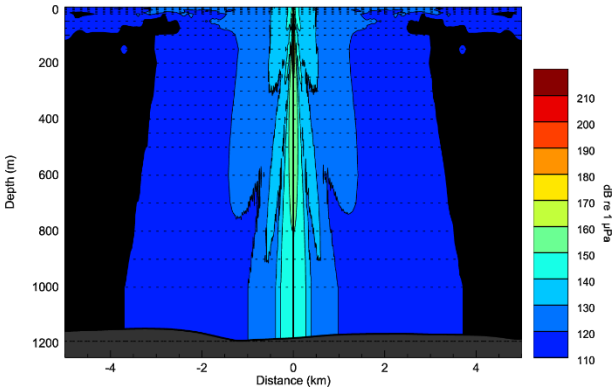

Figure 19. Sub-bottom profiler: Vertical slice of the modelled SPL field at Site S1, February propagation conditions.

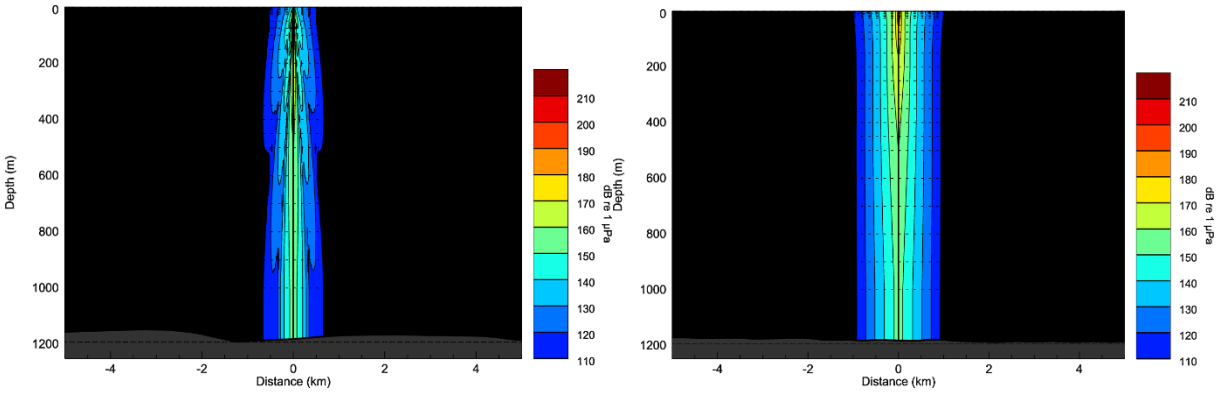

Figure 20. Multi-beam echosounder: Vertical slice along (left) and across (right) the towing track of the modelled SPL field at Site S1, February propagation conditions.

4.2.2. Sound Exposure Levels

The calculations of the SEL for the track used modelled per-pulse SEL fields that were modelled for the sub-bottom profiler and multi-beam echosounder at Site S1 for February propagation conditions.

Sound exposure levels were calculated with the methodology for the Safe Distance estimation for mobile sources and static receivers described in NMFS (2018), but were enhanced to account for the source directivity and propagation environment properties (see Section 2.3).

The Safe Distance (R_{SD}) was estimated for each marine mammal group using M-weighting functions and specific TTS- and PTS-onset thresholds defined in NMFS (2018) for impulsive source. The calculations were performed assuming that the source is engaged every 2 m along the track. Table 11 presents the Safe Distances results.

Table 11. Sub-bottom profiler and multi-beam echosounder: Safe distances in metres to PTS- and TTS-onset thresholds based on the SEL field calculated over a track section.

Marine mammal group	PTS-onset			TTS-onset		
	peak SPL (dB re 1 µPa)	MBES	SBP	peak SPL (dB re 1 µPa)	MBES	SBP
Low-frequency cetaceans	183	<5	<5	168	<5	<5
Mid-frequency cetaceans	185	<5	<5	170	<5	<5
High-frequency cetaceans	155	<5	43	140	11	215
Phocid pinnipeds (underwater)	185	<5	<5	170	<5	<5
Otariid pinnipeds (underwater)	203	<5	<5	188	<5	<5

4.3. Vessels

The vessel operations were modelled at Site S1 (Core Development Area) for two propagation conditions, February and August. The following three scenarios for vessel operations were modelled:

- Drillship (*Stena Carron*),
- FPSO facility, and
- Drillship + FPSO facility.

The source levels were designed to represent operation of the vessels with 50% power output of the dynamic positioning thrusters. The modelling was performed for the frequency range from 10 to 25,000 Hz along 72 transects up to 50 km range from the source. For the simplicity of the interpretation, vessels were represented by a point source. For the multi-vessel scenario, it was assumed that the point sources representing each vessel are located at the same horizontal location but at different depths.

4.3.1. SPL

Vessels are non-impulsive or continuous noise sources. For continuous sources, SPL and SEL are equivalent because the integration time for the purpose of the SPL calculations is taken as constant. Therefore, the SPL field for continuous sources can be estimated using transmission loss modelling approach (Section 2.2.1).

The underwater sound fields predicted by the propagation models were sampled such that the received sound level at each point in the horizontal plane was taken to be the maximum value over all modelled depths for that point (Section 2.2.3). The resultant maximum-over-depth SPL fields are presented below in two formats: as tables of distances to sound levels and as contour maps showing the directivity and range to various sound levels.

The predicted distances to specific levels were computed from the maximum-over-depth sound fields. Two distances, relative to the source, are reported for each sound level: (1) R_{max}, the maximum range at which the given sound level was encountered in the modelled maximum-over-depth sound field, and (2) $R_{95\%}$, the maximum range at which the given sound level was encountered after excluding 5% of the farthest such points.

The distances to the sound level thresholds from 160 to 120 dB re 1 µPa SPL with 10 dB step for all three vessel scenarios at Site S1 are presented in Tables 12 and 13 for February and August propagation conditions, respectively. The contour maps of the estimated acoustic fields in SPL are presented on Figure 21 (February) and Figure 22 (August).

Table 12. Vessels: Maximum (R_{max}, m) and 95% ($R_{95\%}$, m) horizontal distances to modelled maximum-over-depth SPL thresholds at Site S1 for February propagation conditions.

SPL (dB re 1 µPa)	*Stena Carron*		FPSO facility		*Stena Carron* + FPSO	
	R_{max}	$R_{95\%}$	R_{max}	$R_{95\%}$	R_{max}	$R_{95\%}$
160	<40	<40	<40	<40	<40	<40
150	102	102	63	63	122	122
140	335	326	220	213	398	386
130	3270	3210	707	688	5690	5590
120	25500	25100	14000	13700	34000	31000

Table 13. Vessels: Maximum (R_{max}, m) and 95% ($R_{95\%}$, m) horizontal distances to modelled maximum-over-depth SPL thresholds at Site S1 for August propagation conditions.

SPL (dB re 1 µPa)	*Stena Carron*		FPSO facility		*Stena Carron* + FPSO	
	R_{max}	$R_{95\%}$	R_{max}	$R_{95\%}$	R_{max}	$R_{95\%}$
160	<40	<40	<40	<40	<40	<40
150	100	100	63	63	117	117
140	335	326	220	189	416	405
130	1590	1550	990	963	1970	1920
120	7960	5850	3750	3600	10500	7240

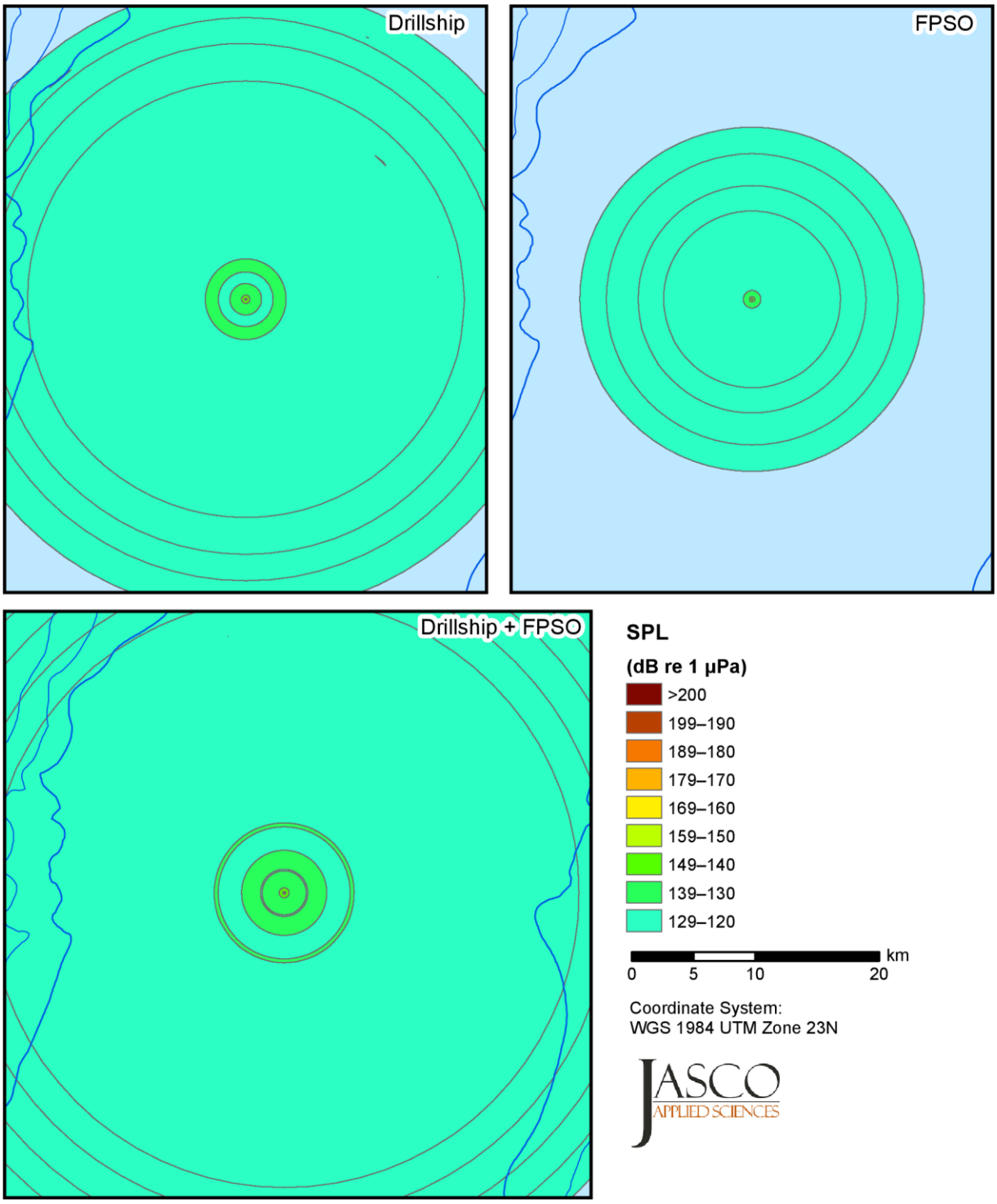

Figure 21. Vessels: Modelled SPL field at Site S1 for February propagation conditions.

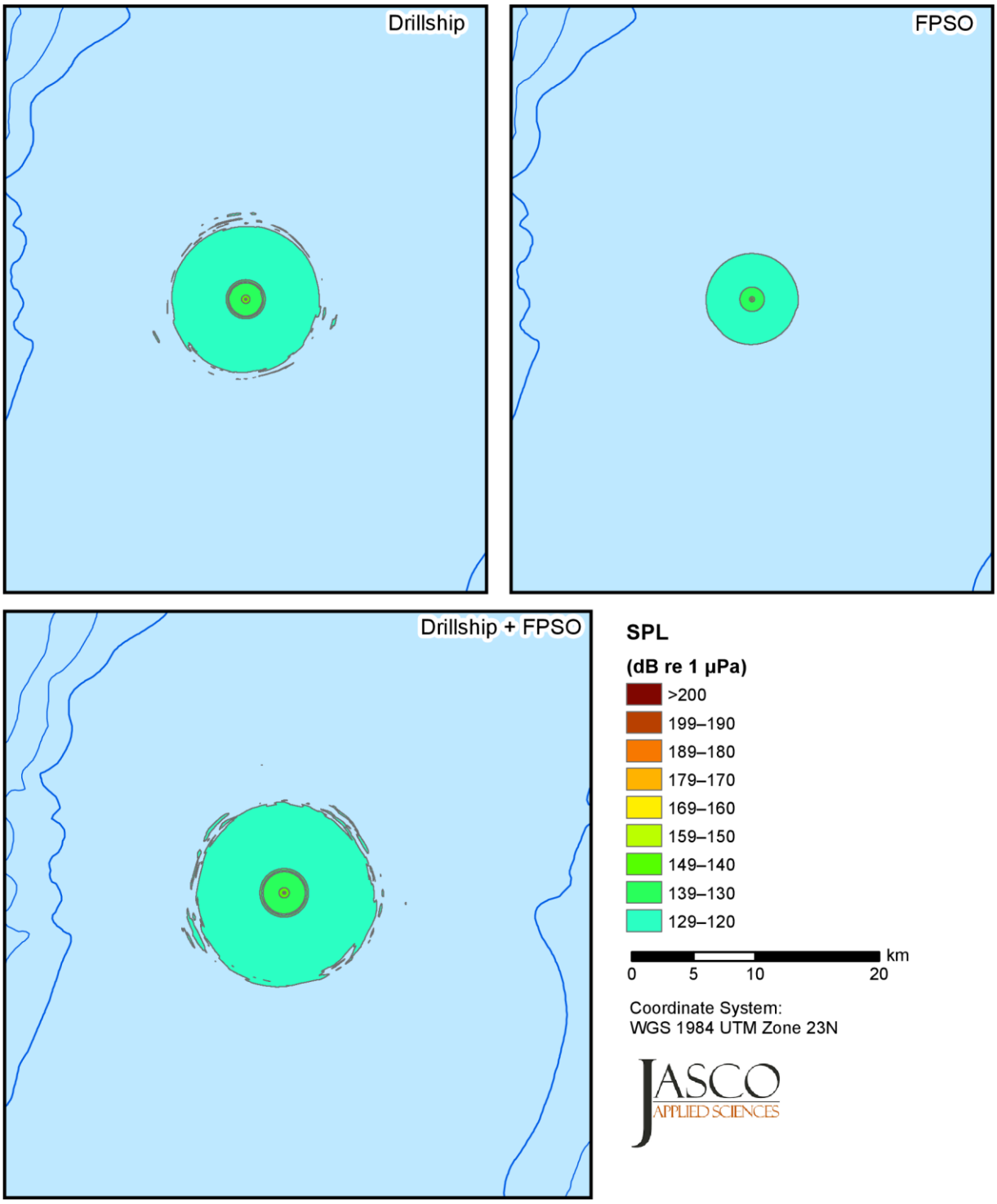

Figure 22. Vessels: Modelled SPL field at Site S1 for August propagation conditions.

4.3.2. Sound Exposure Levels

For the purpose of the 24-hr SEL calculations it was assumed that the vessels are stationary, and the source levels do not change with time. The SEL_{24hr} was estimated from 1 sec SEL by adding 49.3 dB to account for the number of seconds in 24 hours (86,400 seconds).

The maximum ranges to the specific TTS- and PTS-onset thresholds were estimated for each marine mammal group using M-weighting functions as defined in NMFS (2018) for non-impulsive noise source. The calculations were performed for three vessels scenarios at Site S1 for February (Table 14) and August (Table 15) propagation.

Table 14. Vessels: Maximum ranges in metres to PTS- and TTS-onset thresholds based on the 24 hr SEL field (NMFS 2018). February propagation conditions.

Marine mammal group	PTS-onset				TTS-onset			
	SEL_{24hr} (dB re 1 µPa²·s)	*Stena Carron*	FPSO	*Stena Carron* + FPSO	SEL_{24hr} (dB re 1 µPa²·s)	*Stena Carron*	FPSO	*Stena Carron* + FPSO
Low-frequency cetaceans	199	100	60	117	179	3250	684	5610
Mid-frequency cetaceans	198	<40	<40	<40	178	197	122	233
High-frequency cetaceans	173	234	146	280	153	5930	3380	6140
Phocid pinnipeds (underwater)	201	<40	<40	45	181	420	263	497
Otariid pinnipeds (underwater)	219	<40	<40	<40	199	45	<40	57

Table 15. Vessels: Maximum ranges in metres to PTS- and TTS-onset thresholds based on the 24 hr SEL field. August propagation conditions.

Marine mammal group	PTS-onset				TTS-onset			
	SEL_{24hr} (dB re 1 µPa²·s)	*Stena Carron*	FPSO	*Stena Carron* + FPSO	SEL_{24hr} (dB re 1 µPa²·s)	*Stena Carron*	FPSO	*Stena Carron* + FPSO
Low-frequency cetaceans	199	89	57	113	179	1310	691	1960
Mid-frequency cetaceans	198	<40	<40	<40	178	190	117	226
High-frequency cetaceans	173	228	146	281	153	4280	2990	4290
Phocid pinnipeds (underwater)	201	<40	<40	45	181	420	260	525
Otariid pinnipeds (underwater)	219	<40	<40	<40	199	45	<40	57

5. Discussion

The acoustic field modelling was performed for three types of sources: a seismic source (impulsive), geotechnical survey sources (impulsive), and vessels (non-impulsive). The propagation conditions were tested for two months (August and February) that feature different sound speed profiles in the water column. The February sound speed profile features a surface channel without a defined bottom limit that traps some acoustic energy; however, a moderate velocity gradient still allows a significant amount of the acoustic energy to escape towards the bottom (Figure 6). The sound speed profile typical for August features a high negative velocity gradient at the top, which refracts the acoustic wave towards the bottom and prevents it from being trapped in the deep acoustic channel.

The vertical distribution of the acoustic energy is primarily defined by the sound speed profile. In February the acoustic energy tends to concentrate in the top 200 m once the trapping effect of the surface channel start prevailing at ranges more than 10 km. For August propagation conditions, the acoustic energy is uniformly spread through the entire water column without any prominent maximums. The vertical position of the sounds source has no affect on how the acoustic energy is distributed through the water column.

The propagation of the sound along different azimuths depends on the directivity of the source and the topography of the bottom. The source levels of the 5085 in³ seismic array in the 50–80 Hz frequency band are higher in the endfire direction with wide lobes, and in the 160–300 Hz frequency range, the source levels are higher in the broadside direction with much narrower lobes (Figure 9). As a result, the ranges to specific acoustic thresholds are longer for the endfire and broadside directions. The topography defines the spread of the acoustic energy in the vertical dimension. As the water depth increases, the acoustic wave has more space to refract upward without hitting the bottom and losing energy at the bottom interface, as such the transmission loss decreases compared to the profile with constant water depth. For the propagation profiles with decreasing water depth, two effects take place. The decreasing water depth concentrates the acoustic energy within narrower waveguide, which increases the sound levels. Conversely, the acoustic wave interacts with the bottom more often, losing greater fraction of its energy into the sediment. The latter effect prevails, and propagation profiles with decreasing water depths, such as towards the shelf, have higher transmission loss decreases compared to the profile with a constant water depth.

As the acoustic wave reaches the shelf waters (water depths 100–300 m), the transmission loss reaches values of 90–95 dB and the non-weighted SEL decreases to 130–135 dB re 1 µPa²s.

The modelled acoustic fields were tested against various impact criteria defined in terms of a single event, per-pulse in case of impulsive sources and per-second for non-impulsive sources, and continuous source operation for a specific time period.

The ranges to the acoustic thresholds defined in terms of peak SPL were greater than 100 m only for high-frequency cetaceans (Table 7). The acoustic thresholds levels for all other groups are at least 17 dB higher (and up to 30 dB higher); therefore, the ranges to the thresholds are much smaller (less than 40 m). It should be noted that both SPL and peak SPL signal metric is calculated based on the non-weighted broad band signal, i.e., the hearing frequency band of specific marine mammals is not taken into account, and M-weighting functions are not applied in this case. As such, a multi-beam echosounder operating at 200 Hz can affect the hearing of the high-frequency cetaceans up to a distance 160 m from the source according to the criteria defined in terms of the peak SPL (Table 7).

While comparing the ranges to specific acoustic thresholds for the vessels modelled at various locations along the Canadian Atlantic coast, the modelled ranges are higher for the vessels operating offshore Nova Scotia. This is because the sound speed profile in the water column for the offshore Nova Scotia area features more prominent surface channel with higher vertical gradient and larger speed difference between the minimum value at the top and maximum value at the bottom. Such channel traps greater portion of the acoustic energy released by the source and conveys it to longer ranges with lower transmission loss compared to the propagation conditions in the region considered in this report.

Literature Cited

[ISO] International Organization for Standardization. 2017. *ISO 18405.2:2017. Underwater acoustics—Terminology*. Geneva. https://www.iso.org/obp/ui/#iso:std:iso:18405:ed-1:v1:en.

[ITC] International Transducer Corporation. 1993. *Application Equations for Underwater Sound Transducers* (pamphlet). International Transducer Corporation, Santa Barbara, CA.

[NMFS] National Marine Fisheries Service. 2016. *Technical Guidance for Assessing the Effects of Anthropogenic Sound on Marine Mammal Hearing: Underwater Acoustic Thresholds for Onset of Permanent and Temporary Threshold Shifts*. U.S. Department of Commerce, NOAA. NOAA Technical Memorandum NMFS-OPR-55. 178 pp.

[NMFS] National Marine Fisheries Service. 2018. *2018 Revision to: Technical Guidance for Assessing the Effects of Anthropogenic Sound on Marine Mammal Hearing (Version 2.0): Underwater Thresholds for Onset of Permanent and Temporary Threshold Shifts*. U.S. Department of Commerce, NOAA. NOAA Technical Memorandum NMFS-OPR-59. 167 pp. https://www.fisheries.noaa.gov/webdam/download/75962998.

Aerts, L., M. Blees, S.B. Blackwell, C.R. Greene, Jr., K. Kim, D.E. Hannay, and M. Austin. 2008. *Marine mammal monitoring and mitigation during BP Liberty OBC seismic survey in Foggy Island Bay, Beaufort Sea, July-August 2008: 90-day report*. Document Number LGL Report P1011-1. Report by LGL Alaska Research Associates Inc., LGL Ltd., Greeneridge Sciences Inc. and JASCO Applied Sciences for BP Exploration Alaska. 199 pp. http://www.nmfs.noaa.gov/pr/pdfs/permits/bp_liberty_monitoring.pdf.

ANSI S1.1-2013. R2013. *American National Standard Acoustical Terminology*. American National Standards Institute, New York.

Becker, J.J., D.T. Sandwell, W.H.F. Smith, J. Braud, B. Binder, J. Depner, D. Fabre, J. Factor, S. Ingalls, et al. 2009. Global Bathymetry and Elevation Data at 30 Arc Seconds Resolution: SRTM30_PLUS. *Marine Geodesy* 32(4): 355-371.

Buckingham, M.J. 2005. Compressional and shear wave properties of marine sediments: Comparisons between theory and data. *Journal of the Acoustical Society of America* 117(1): 137-152. http://dx.doi.org/10.1121/1.1810231.

Carnes, M.R. 2009. *Description and Evaluation of GDEM-V 3.0*. Document Number NRL Memorandum Report 7330-09-9165. U.S. Naval Research Laboratory, Stennis Space Center, MS. 21 pp.

Černý, V. 1985. Thermodynamical approach to the traveling salesman problem: An efficient simulation algorithm. *Journal of Optimization Theory and Applications* 45: 41-51.

Collins, M.D. 1993. A split-step Padé solution for the parabolic equation method. *Journal of the Acoustical Society of America* 93(4): 1736-1742. https://doi.org/10.1121/1.406739.

Collins, M.D., R.J. Cederberg, D.B. King, and S. Chin-Bing. 1996. Comparison of algorithms for solving parabolic wave equations. *Journal of the Acoustical Society of America* 100(1): 178-182. https://doi.org/10.1121/1.415921.

Coppens, A.B. 1981. Simple equations for the speed of sound in Neptunian waters. *Journal of the Acoustical Society of America* 69(3): 862-863. http://dx.doi.org/10.1121/1.385486.

Dragoset, W.H. 1984. A comprehensive method for evaluating the design of airguns and airgun arrays. *Proceedings, 16th Annual Offshore Technology Conference* Volume 3, 7-9 May 1984. OTC 4747, Houston, TX. pp 75–84.

Finneran, J.J. 2015. *Auditory weighting functions and TTS/PTS exposure functions for cetaceans and marine carnivores*. Technical report by SSC Pacific, San Diego, CA.

Finneran, J.J. 2016. *Auditory weighting functions and TTS/PTS exposure functions for marine mammals exposed to underwater noise*. Technical Report for Space and Naval Warfare Systems Center Pacific, San Diego, CA. 49 pp. http://www.dtic.mil/dtic/tr/fulltext/u2/1026445.pdf.

Fisher, F.H. and V.P. Simmons. 1977. Sound absorption in sea water. *Journal of the Acoustical Society of America* 62(3): 558-564. https://doi.org/10.1121/1.381574.

Funk, D., D.E. Hannay, D.S. Ireland, R. Rodrigues, and W.R. Koski (eds.). 2008. *Marine mammal monitoring and mitigation during open water seismic exploration by Shell Offshore Inc. in the Chukchi and Beaufort Seas, July–November 2007: 90-day report*. LGL Report P969-1. Prepared by LGL Alaska Research Associates Inc., LGL Ltd., and JASCO Research Ltd. for Shell Offshore Inc., National Marine Fisheries Service (U.S.), and U.S. Fish and Wildlife Service. 218 pp.

Hannay, D.E. and R.G. Racca. 2005. *Acoustic Model Validation*. Document Number 0000-S-90-04-T-7006-00-E, Revision 02. Technical report by JASCO Research Ltd. for Sakhalin Energy Investment Company Ltd. 34 pp.

Ireland, D.S., R. Rodrigues, D. Funk, W.R. Koski, and D.E. Hannay. 2009. *Marine mammal monitoring and mitigation during open water seismic exploration by Shell Offshore Inc. in the Chukchi and Beaufort Seas, July–October 2008: 90-Day Report*. Document Number LGL Report P1049-1. 277 pp.

Kinsler, L.E., A.R. Frey, A.B. Coppens, and J.V. Sanders. 1950. *Fundamentals of acoustics*. John Wiley & Sons Inc., New York.

Landro, M. 1992. Modeling of GI gun signatures. *Geophysical Prospecting* 40: 721–747. https://doi.org/10.1111/j.1365-2478.1992.tb00549.x

Laws, R.M., L. Hatton, and M. Haartsen. 1990. Computer modeling of clustered airguns. *First Break* 8(9): 331–338.

Lurton, X. 2002. *An Introduction to Underwater Acoustics: Principles and Applications*. Springer, Chichester, UK. 347 pp.

MacGillivray, A.O. and N.R. Chapman. 2012. Modeling underwater sound propagation from an airgun array using the parabolic equation method. *Canadian Acoustics* 40(1): 19-25. http://jcaa.caa-aca.ca/index.php/jcaa/article/view/2502.

Martin, B., K. Broker, M.-N.R. Matthews, J. MacDonnell, and L. Bailey. 2015. *Comparison of measured and modeled air-gun array sound levels in Baffin Bay, West Greenland. OceanNoise 2015*, 11-15 May, Barcelona, Spain.

Massa, D.P. 2003. Acoustic transducers. *In Wiley Encyclopedia of Telecommunications*. John Wiley & Sons, Inc. http://dx.doi.org/10.1002/0471219282.eot136.

McPherson, C.R., M. Wood, and R.G. Racca. 2016. *Impacts of Noise from FPSO Facility Operations on Marine Fauna, ConocoPhillips Barossa Field*. Document Number 01117, Version 1.0. Technical report by JASCO Applied Sciences for Jacobs.

O'Neill, C., D. Leary, and A. McCrodan. 2010. Sound Source Verification. (Chapter 3) *In* Blees, M.K., K.G. Hartin, D.S. Ireland, and D.E. Hannay (eds.). *Marine mammal monitoring and mitigation during open water seismic exploration by Statoil USA E&P Inc. in the Chukchi Sea, August-October 2010: 90-day report*. LGL Report P1119. Prepared by LGL Alaska Research Associates Inc., LGL Ltd., and JASCO Applied Sciences Ltd. for Statoil USA E&P Inc., National Marine Fisheries Service (U.S.), and U.S. Fish and Wildlife Service. pp 1-34.

Porter, M.B. and Y.-C. Liu. 1994. Finite-element ray tracing. *In*: Lee, D. and M.H. Schultz (eds.). *Proceedings of the International Conference on Theoretical and Computational Acoustics*. Volume 2. World Scientific Publishing Co. pp 947-956.

Racca, R.G. and J.A. Scrimger. 1986. *Underwater Acoustic Source Characteristics of Air and Water Guns*. Document Number DREP Tech. Rep. 06SB 97708-5-7055. Report by JASCO Research Ltd. for Defence Research Establishment Pacific (Canada), Victoria, BC.

Racca, R.G., A. Rutenko, K. Bröker, and M. Austin. 2012a. A line in the water - design and enactment of a closed loop, model based sound level boundary estimation strategy for mitigation of behavioural impacts from a seismic survey. *11th European Conference on Underwater Acoustics 2012*. Volume 34(3), Edinburgh, United Kingdom.

Racca, R.G., A. Rutenko, K. Bröker, and G. Gailey. 2012b. *Model based sound level estimation and in-field adjustment for real-time mitigation of behavioural impacts from a seismic survey and post-event evaluation of sound exposure for individual whales*. *Acoustics 2012 Fremantle: Acoustics, Development and the Environment*, Fremantle, Australia. http://www.acoustics.asn.au/conference_proceedings/AAS2012/papers/p92.pdf.

Smith, W.H.F. and D.T. Sandwell. 1997. Global sea floor topography from satellite altimetry and ship depth soundings. *Science* 277(5334): 1956-1962.

Southall, B.L., A.E. Bowles, W.T. Ellison, J.J. Finneran, R.L. Gentry, C.R. Greene, Jr., D. Kastak, D.R. Ketten, J.H. Miller, et al. 2007. Marine Mammal Noise Exposure Criteria: Initial Scientific Recommendations. *Aquatic Mammals* 33(4): 411-521. https://doi.org/10.1080/09524622.2008.9753846.

Teague, W.J., M.J. Carron, and P.J. Hogan. 1990. A comparison between the Generalized Digital Environmental Model and Levitus climatologies. *Journal of Geophysical Research* 95(C5): 7167-7183.

Warner, G.A., C. Erbe, and D.E. Hannay. 2010. Underwater Sound Measurements. (Chapter 3) *In* Reiser, C.M., D. Funk, R. Rodrigues, and D.E. Hannay (eds.). *Marine Mammal Monitoring and Mitigation during Open Water Shallow Hazards and Site Clearance Surveys by Shell Offshore Inc. in the Alaskan Chukchi Sea, July-October 2009: 90-Day Report*. LGL Report P1112-1. Report by LGL Alaska Research Associates Inc. and JASCO Applied Sciences for Shell Offshore Inc., National Marine Fisheries Service (U.S.), and U.S. Fish and Wildlife Service. pp 1-54.

Zhang, Z.Y. and C.T. Tindle. 1995. Improved equivalent fluid approximations for a low shear speed ocean bottom. *Journal of the Acoustical Society of America* 98(6): 3391-3396. https://doi.org/10.1121/1.413789.

Ziolkowski, A. 1970. A method for calculating the output pressure waveform from an airgun. *Geophysical Journal of the Royal Astronomical Society* 21(2): 137-161. https://doi.org/10.1111/j.1365-246X.1970.tb01773.x.

Appendix A. Signal Levels at Specific Ranges from the Seismic Source

The signal levels at specific ranges from the seismic source were retrieved from the output of the full waveform modelling. The signal levels included SPL (L_p), peak SPL ($L_{p,pk}$), and SEL (L_E), calculated directly from the modelled synthetic pressure waveforms. The full waveform modelling was performed for two propagation conditions and along five profiles at each of the two sites.

Signal levels for February and August propagation conditions at Site S1 are listed in Table A-1 and for Site S2 in Table A-2. At each horizontal range along each modelled profile, the levels are reported at three depths: the receivers with the highest SPL (L_p) and highest peak SPL ($L_{p,pk}$) are found across the water column and for the deepest receiver within the water column ("bottom"). Column "depth" indicates the vertical position of the modelled receivers in the case of maximum L_p and $L_{p,pk}$ and bottom depth for the "bottom" case. For each selected receiver, three signal levels are reported: L_p , $L_{p,pk}$, and per-pulse sound exposure level (L_E). In the case of L_p and $L_{p,pk}$ maximums occurring at the same depth, the same set of levels are repeated.

Table A-1. Site S1: Signal levels at specific ranges from the seismic source for February and August propagation conditions.

Range (m)	Azimuth (°)	Max metric	February				August			
			Depth (m)	L_p (dB re 1 µPa)	$L_{p,pk}$ (dB re 1 µPa)	L_E (dB re 1 µPa²s)	Depth (m)	L_p (dB re 1 µPa)	$L_{p,pk}$ (dB re 1 µPa)	L_E (dB re 1 µPa²s)
50	123	L_p	50	201.2	210.5	191.9	50	201.1	210.6	191.7
		$L_{p,pk}$	25	200.6	211.3	191.2	25	200.3	211.1	190.8
		Bottom	1182	184.4	192.9	175.6	1182	184.5	193.2	175.7
	180	L_p	10	200.0	212.3	190.1	50	199.9	212.3	190.4
		$L_{p,pk}$	20	198.4	213.8	188.8	25	198.8	213.5	189.2
		Bottom	1182	182.5	191.5	173.6	1182	182.5	191.6	173.6
	202	L_p	50	198.9	208.9	189.4	50	198.7	208.8	189.2
		$L_{p,pk}$	25	198.0	209.4	188.4	25	197.6	209.5	188.1
		Bottom	1181	182.5	191.6	173.5	1181	182.5	191.7	173.6
	270	L_p	50	200.6	210.0	191.0	50	200.4	210.5	190.9
		$L_{p,pk}$	20	200.0	213.2	190.2	25	200.3	212.9	190.6
		Bottom	1181	183.5	193.3	174.5	1181	183.6	193.5	174.5
	352	L_p	50	199.4	211.1	189.9	50	199.4	211.4	189.9
		$L_{p,pk}$	25	198.8	212.4	189.2	25	198.4	212.6	188.8
		Bottom	1181	182.4	191.6	173.5	1181	182.5	191.5	173.5
500	123	L_p	350	181.6	192.0	172.2	350	181.5	192.1	172.1
		$L_{p,pk}$	250	180.9	192.1	171.4	300	181.2	192.2	171.7
		Bottom	1184	177.6	186.7	168.5	1184	177.6	186.8	168.6
	180	L_p	350	181.0	192.9	171.4	150	181.0	193.6	171.2
		$L_{p,pk}$	200	178.6	193.5	168.9	150	181.0	193.6	171.2
		Bottom	1185	176.7	186.8	167.3	1185	176.6	187.3	167.3
	202	L_p	350	179.1	188.6	169.7	350	179.0	188.8	169.6
		$L_{p,pk}$	250	178.2	189.1	168.6	250	177.8	189.2	168.2
		Bottom	1184	175.8	185.2	166.5	1184	175.8	185.1	166.5
	270	L_p	300	180.9	192.5	171.3	300	180.9	192.8	171.2
		$L_{p,pk}$	200	180.4	193.8	170.7	200	180.0	193.5	170.4
		Bottom	1180	177.1	185.4	167.7	1180	177.1	185.5	167.7

Range (m)	Azimuth (°)	Max metric	February				August			
			Depth (m)	L_p (dB re 1 µPa)	$L_{p,pk}$ (dB re 1 µPa)	L_E (dB re 1 µPa²s)	Depth (m)	L_p (dB re 1 µPa)	$L_{p,pk}$ (dB re 1 µPa)	L_E (dB re 1 µPa²s)
1000	352	L_p	300	180.0	191.9	170.4	400	180.0	191.4	170.5
		$L_{p,pk}$	250	179.2	192.2	169.6	200	178.5	192.4	168.9
		Bottom	1174	176.4	186.9	166.9	1174	176.3	186.3	166.9
	123	L_p	700	175.4	185.6	166.2	800	175.3	185.5	166.1
		$L_{p,pk}$	500	174.9	186.0	165.6	600	175.1	186.1	165.9
		Bottom	1185	175.0	184.8	165.9	1185	175.0	184.9	165.9
	180	L_p	600	174.7	187.0	165.2	250	175.3	188.1	165.5
		$L_{p,pk}$	250	174.0	187.2	164.3	250	175.3	188.1	165.5
		Bottom	1189	173.7	183.6	164.4	1189	173.8	184.1	164.5
	202	L_p	800	172.9	182.3	163.6	800	172.8	182.8	163.5
		$L_{p,pk}$	600	172.7	183.0	163.4	450	171.4	183.2	162.1
		Bottom	1183	172.7	181.7	163.6	1183	172.6	181.8	163.5
	270	L_p	600	174.9	186.4	165.4	700	174.9	185.9	165.4
		$L_{p,pk}$	400	174.4	187.6	164.8	500	174.6	187.6	165.1
		Bottom	1180	174.3	184.7	165.1	1180	174.4	184.6	165.1
	352	L_p	700	174.1	185.5	164.6	250	174.1	185.7	164.3
		$L_{p,pk}$	450	172.7	186.1	163.3	300	173.9	186.5	164.2
		Bottom	1168	173.2	183.3	164.0	1168	173.2	183.4	164.0
10000	123	L_p	15	156.7	166.7	148.5	20	156.7	166.7	148.1
		$L_{p,pk}$	15	156.7	166.7	148.5	20	156.7	166.7	148.1
		Bottom	1173	155.0	165.0	148.7	1173	154.1	164.7	147.2
	180	L_p	50	163.1	174.4	153.9	10	159.8	171.1	150.2
		$L_{p,pk}$	50	163.1	174.4	153.9	10	159.8	171.1	150.2
		Bottom	1170	156.1	165.9	148.6	1170	154.9	167.5	148.1
	202	L_p	25	155.6	164.4	147.8	25	155.5	164.2	147.0
		$L_{p,pk}$	15	154.5	164.6	146.5	15	154.0	165.2	145.5
		Bottom	1167	152.6	161.0	145.6	1167	152.0	161.0	144.9
	270	L_p	50	156.7	169.0	150.2	20	155.6	166.4	148.0
		$L_{p,pk}$	75	156.6	169.9	149.9	15	155.5	167.6	147.6
		Bottom	1155	155.9	165.3	148.5	1155	155.5	165.2	147.4
	352	L_p	50	161.5	173.5	153.0	100	159.0	171.7	150.1
		$L_{p,pk}$	50	161.5	173.5	153.0	100	159.0	171.7	150.1
		Bottom	1158	154.9	165.0	147.9	1158	154.3	165.0	147.1
25000	123	L_p	75	149.5	157.8	143.6	50	147.0	155.2	141.6
		$L_{p,pk}$	250	147.8	158.7	143.1	20	146.4	158.0	140.9
		Bottom	1032	147.1	158.4	142.3	1032	146.1	155.4	141.2
	180	L_p	20	158.0	170.6	148.9	15	149.7	161.8	142.1
		$L_{p,pk}$	20	158.0	170.6	148.9	10	148.9	162.3	142.5
		Bottom	1164	147.6	158.6	141.9	1164	148.9	158.9	142.5
	202	L_p	150	148.4	158.2	142.1	25	145.0	155.2	139.2
		$L_{p,pk}$	150	148.4	158.2	142.1	400	144.2	156.4	140.1
		Bottom	1174	143.8	152.1	139.2	1174	143.4	150.9	138.2
	270	L_p	75	152.2	161.3	145.1	15	147.4	158.9	141.4
		$L_{p,pk}$	15	150.8	165.7	144.7	25	147.0	159.6	141.9

Range (m)	Azimuth (°)	Max metric	February				August			
			Depth (m)	L_p (dB re 1 µPa)	$L_{p,pk}$ (dB re 1 µPa)	L_E (dB re 1 µPa²s)	Depth (m)	L_p (dB re 1 µPa)	$L_{p,pk}$ (dB re 1 µPa)	L_E (dB re 1 µPa²s)
50000		Bottom	824	147.7	158.7	140.7	824	145.9	157.0	139.6
	352	L_p	20	155.9	165.7	147.1	1000	152.5	163.2	144.5
		$L_{p,pk}$	75	154.2	167.6	146.0	1000	152.5	163.2	144.5
		Bottom	1050	150.6	160.4	143.5	1050	152.5	163.2	144.5
	123	L_p	50	145.3	150.5	138.7	100	140.6	147.9	134.4
		$L_{p,pk}$	300	142.2	153.4	136.6	20	137.5	149.0	132.1
		Bottom	406	138.1	151.0	135.2	406	136.1	146.2	132.5
	180	L_p	25	154.0	165.8	145.0	10	144.0	156.2	137.6
		$L_{p,pk}$	25	154.0	165.8	145.0	15	143.9	156.6	137.5
		Bottom	1103	141.8	153.2	136.3	1103	139.7	149.5	135.7
	202	L_p	50	143.5	154.1	139.0	100	142.1	149.9	135.1
		$L_{p,pk}$	50	143.5	154.1	139.0	100	142.1	149.9	135.1
		Bottom	1166	138.4	146.7	134.7	1166	137.1	144.9	134.0
	270	L_p	50	149.2	160.3	140.9	75	140.5	147.7	133.5
		$L_{p,pk}$	50	149.2	160.3	140.9	15	135.7	148.8	130.2
		Bottom	487	138.4	149.6	133.4	487	136.6	147.4	131.7
	352	L_p	50	151.2	161.8	142.9	900	141.3	152.7	134.0
		$L_{p,pk}$	50	151.2	161.8	142.9	900	141.3	152.7	134.0
		Bottom	1797	141.6	154.4	135.3	1797	139.3	150.7	134.1
100000	123	L_p	75	141.0	146.6	133.8	100	138.0	144.5	128.8
		$L_{p,pk}$	50	140.4	147.4	133.8	100	138.0	144.5	128.8
		Bottom	254	133.2	139.4	125.7	254	126.4	132.7	120.9
	180	L_p	20	149.7	160.5	141.7	75	134.6	143.1	128.7
		$L_{p,pk}$	50	149.7	160.8	141.6	75	134.6	143.1	128.7
		Bottom	360	142.4	153.8	134.8	360	129.8	139.2	125.6
	202	L_p	50	139.3	148.4	133.2	75	133.8	141.2	128.6
		$L_{p,pk}$	50	139.3	148.4	133.2	75	133.8	141.2	128.6
		Bottom	1172	133.3	141.8	128.5	1172	131.5	139.7	126.6
	270	L_p	15	143.8	154.6	135.4	100	135.0	141.2	128.4
		$L_{p,pk}$	15	143.8	154.6	135.4	100	135.0	141.2	128.4
		Bottom	340	140.1	150.0	131.1	340	130.4	139.6	124.3
	352	L_p	50	147.8	159.5	140.5	1400	141.1	154.8	132.3
		$L_{p,pk}$	50	147.8	159.5	140.5	1400	141.1	154.8	132.3
		Bottom	2726	133.8	146.0	127.5	2726	135.9	148.4	128.3
150000	123	L_p	75	139.0	144.4	131.2	75	133.7	142.5	124.5
		$L_{p,pk}$	50	138.5	144.6	131.2	75	133.7	142.5	124.5
		Bottom	170	132.9	140.5	125.8	170	127.9	135.5	120.0
	180	L_p	25	147.9	159.4	139.1	100	130.6	137.9	124.4
		$L_{p,pk}$	25	147.9	159.4	139.1	100	130.6	137.9	124.4
		Bottom	355	129.8	140.4	125.0	355	120.7	129.7	116.4
	202	L_p	50	138.4	149.0	131.7	700	130.3	134.9	124.7
		$L_{p,pk}$	50	138.4	149.0	131.7	600	130.2	137.5	124.1
		Bottom	1049	132.5	145.6	126.8	1049	127.6	136.2	123.2
	270	L_p	50	142.1	150.7	134.5	100	132.8	138.2	125.5

Range (m)	Azimuth (°)	Max metric	February				August			
			Depth (m)	L_p (dB re 1 µPa)	$L_{p,pk}$ (dB re 1 µPa)	L_E (dB re 1 µPa²s)	Depth (m)	L_p (dB re 1 µPa)	$L_{p,pk}$ (dB re 1 µPa)	L_E (dB re 1 µPa²s)
		$L_{p,pk}$	50	142.1	150.7	134.5	100	132.8	138.2	125.5
		Bottom	276	134.7	144.8	127.6	276	125.9	132.9	120.4
	352	L_p	50	145.9	157.4	138.1	15	136.9	148.3	128.1
		$L_{p,pk}$	50	145.9	157.4	138.1	900	136.5	149.7	128.6
		Bottom	2832	127.8	138.8	123.6	2832	130.2	141.4	124.2

Table A-2. Site S2: Signal levels at specific ranges from the seismic source for February and August propagation conditions.

Range (m)	Azimuth (°)	Max metric	February				August			
			Depth (m)	L_p (dB re 1 µPa)	$L_{p,pk}$ (dB re 1 µPa)	L_E (dB re 1 µPa²s)	Depth (m)	L_p (dB re 1 µPa)	$L_{p,pk}$ (dB re 1 µPa)	L_E (dB re 1 µPa²s)
50	102	L_p	50	201.9	212.5	192.6	50	201.8	212.2	192.5
		$L_{p,pk}$	25	201.8	213.0	192.3	25	201.5	213.0	192.0
		Bottom	515	186.3	195.9	177.3	515	186.4	196.0	177.4
	180	L_p	10	200.0	212.3	190.1	50	199.9	212.3	190.3
		$L_{p,pk}$	20	198.5	213.8	188.8	25	198.9	213.5	189.3
		Bottom	514	183.8	194.2	174.5	514	183.8	194.1	174.5
	191	L_p	50	199.2	210.9	189.7	50	199.1	210.7	189.6
		$L_{p,pk}$	25	198.6	211.9	189.0	25	198.2	211.8	188.6
		Bottom	514	183.6	193.9	174.3	514	183.6	193.8	174.3
	237	L_p	50	200.2	210.5	190.6	50	200.1	210.5	190.5
		$L_{p,pk}$	25	199.7	210.6	190.1	50	200.1	210.5	190.5
		Bottom	512	184.5	192.5	175.1	512	184.6	192.9	175.2
	354	L_p	50	199.6	211.6	190.1	50	199.6	212.0	190.0
		$L_{p,pk}$	25	199.0	213.2	189.4	20	198.0	212.6	188.3
		Bottom	513	183.7	193.9	174.4	513	183.6	193.4	174.4
500	102	L_p	350	182.3	192.9	173.2	350	182.2	192.6	173.1
		$L_{p,pk}$	400	182.2	193.1	173.2	400	182.1	192.9	173.1
		Bottom	533	182.0	192.9	172.7	533	182.0	192.8	172.7
	180	L_p	350	180.8	192.6	171.3	150	181.0	193.6	171.3
		$L_{p,pk}$	200	178.6	193.5	169.2	150	181.0	193.6	171.3
		Bottom	519	179.3	191.1	169.7	519	179.5	190.6	169.9
	191	L_p	350	179.8	190.6	170.4	450	179.7	190.3	170.2
		$L_{p,pk}$	200	177.9	191.4	168.6	250	178.4	191.6	169.1
		Bottom	516	178.1	189.7	168.6	516	178.2	189.5	168.7
	237	L_p	500	181.1	191.3	171.6	500	181.0	191.5	171.6
		$L_{p,pk}$	300	180.4	191.9	171.0	350	180.4	191.7	170.8
		Bottom	502	181.1	191.3	171.6	502	181.0	191.5	171.6
	354	L_p	350	180.4	192.0	170.8	350	180.3	192.3	170.7
		$L_{p,pk}$	200	178.3	192.4	169.0	200	178.8	193.0	169.4
		Bottom	505	180.0	190.5	170.6	505	180.1	190.7	170.6
1000	102	L_p	450	176.5	186.1	167.2	450	176.2	186.4	166.9
		$L_{p,pk}$	350	174.9	186.2	166.7	400	175.3	186.6	166.1
		Bottom	539	176.4	186.2	167.1	539	176.2	186.4	166.8
	180	L_p	200	174.4	186.5	165.0	250	175.3	187.9	165.8
		$L_{p,pk}$	500	173.7	187.1	164.3	250	175.3	187.9	165.8
		Bottom	523	173.7	187.1	164.3	523	172.7	187.5	163.3
	191	L_p	450	173.4	184.7	164.0	450	173.0	185.1	163.6
		$L_{p,pk}$	500	172.6	185.6	163.3	500	172.1	185.8	162.8
		Bottom	518	172.6	185.6	163.3	518	172.1	185.8	162.8
	237	L_p	450	174.4	184.7	164.8	450	174.0	184.3	164.4
		$L_{p,pk}$	450	174.4	184.7	164.8	450	174.0	184.3	164.4
		Bottom	496	174.4	184.7	164.8	496	174.0	184.3	164.4

Range (m)	Azimuth (°)	Max metric	February				August			
			Depth (m)	L_p (dB re 1 µPa)	$L_{p,pk}$ (dB re 1 µPa)	L_E (dB re 1 µPa²s)	Depth (m)	L_p (dB re 1 µPa)	$L_{p,pk}$ (dB re 1 µPa)	L_E (dB re 1 µPa²s)
10000	354	L_p	200	173.5	185.9	164.3	250	174.5	186.7	165.0
		$L_{p,pk}$	400	173.3	186.5	164.1	350	173.7	187.0	164.3
		Bottom	498	173.5	186.4	164.0	498	173.0	186.5	163.5
	102	L_p	75	157.9	168.7	152.6	25	157.0	168.9	151.2
		$L_{p,pk}$	75	157.9	168.7	152.6	25	157.0	168.9	151.2
		Bottom	685	155.8	166.2	150.8	685	155.1	166.1	149.9
	180	L_p	50	163.6	174.8	154.9	15	159.6	171.0	151.2
		$L_{p,pk}$	50	163.6	174.8	154.9	10	159.0	171.3	151.1
		Bottom	571	156.7	168.3	150.9	571	156.5	167.7	150.8
	191	L_p	50	160.2	171.4	152.5	15	157.3	169.3	149.7
		$L_{p,pk}$	50	160.2	171.4	152.5	15	157.3	169.3	149.7
		Bottom	517	155.4	167.0	150.5	517	156.0	167.0	149.9
	237	L_p	20	156.1	166.4	149.2	300	155.3	165.1	148.0
		$L_{p,pk}$	300	156.0	166.7	149.2	300	155.3	165.1	148.0
		Bottom	384	155.6	165.2	149.1	384	155.0	163.0	148.1
	354	L_p	50	162.4	173.7	153.8	10	157.0	170.5	149.9
		$L_{p,pk}$	50	162.4	173.7	153.8	10	157.0	170.5	149.9
		Bottom	519	157.7	169.8	151.3	519	155.5	168.0	150.8
25000	102	L_p	75	152.0	160.1	144.9	900	149.1	159.7	144.6
		$L_{p,pk}$	700	150.8	164.2	146.0	900	149.1	159.7	144.6
		Bottom	948	150.3	160.6	145.7	948	149.1	159.7	144.6
	180	L_p	20	158.1	170.6	148.8	700	152.1	163.5	145.8
		$L_{p,pk}$	20	158.1	170.6	148.8	700	152.1	163.5	145.8
		Bottom	708	151.0	163.1	145.3	708	152.1	163.5	145.8
	191	L_p	25	154.8	165.0	146.0	300	147.3	157.1	142.5
		$L_{p,pk}$	20	154.5	165.1	145.6	500	147.2	159.2	142.3
		Bottom	553	147.3	158.9	142.8	553	147.2	159.2	142.3
	237	L_p	50	149.3	156.5	142.0	100	145.4	153.6	139.1
		$L_{p,pk}$	50	149.3	156.5	142.0	100	145.4	153.6	139.1
		Bottom	343	145.2	153.5	140.2	343	141.4	151.2	138.1
	354	L_p	20	156.7	168.4	147.3	450	147.7	159.3	142.4
		$L_{p,pk}$	25	156.7	168.5	147.3	500	147.5	159.9	142.2
		Bottom	824	144.5	156.1	140.7	824	144.9	155.7	141.3
50000	102	L_p	600	148.2	160.8	141.5	500	145.3	154.5	139.2
		$L_{p,pk}$	600	148.2	160.8	141.5	1000	145.2	156.8	139.7
		Bottom	1174	146.1	156.5	139.8	1174	145.2	156.8	139.7
	180	L_p	50	153.6	165.4	145.0	900	145.4	158.1	139.6
		$L_{p,pk}$	50	153.6	165.4	145.0	900	145.4	158.1	139.6
		Bottom	1058	143.3	156.4	138.3	1058	144.1	155.8	138.2
	191	L_p	50	149.9	160.4	142.0	600	143.1	154.0	137.0
		$L_{p,pk}$	50	149.9	160.4	142.0	600	143.1	154.0	137.0
		Bottom	611	143.1	155.6	137.7	611	143.1	154.0	137.0
	237	L_p	150	144.4	152.9	136.3	75	140.3	148.7	132.8
		$L_{p,pk}$	150	144.4	152.9	136.3	75	140.3	148.7	132.8

Range (m)	Azimuth (°)	Max metric	February				August			
			Depth (m)	L_p (dB re 1 µPa)	$L_{p,pk}$ (dB re 1 µPa)	L_E (dB re 1 µPa²s)	Depth (m)	L_p (dB re 1 µPa)	$L_{p,pk}$ (dB re 1 µPa)	L_E (dB re 1 µPa²s)
		Bottom	283	141.1	148.5	134.4	283	135.5	141.7	130.2
	354	L_p	50	152.1	163.3	144.0	200	144.1	158.1	135.6
		$L_{p,pk}$	50	152.1	163.3	144.0	200	144.1	158.1	135.6
		Bottom	1942	137.5	144.5	130.4	1942	138.2	146.2	130.7
100000	102	L_p	300	145.0	157.6	137.3	75	140.9	148.0	134.6
		$L_{p,pk}$	300	145.0	157.6	137.3	10	135.5	149.1	129.5
		Bottom	317	145.0	157.6	137.3	317	137.2	145.5	133.0
	180	L_p	20	149.6	160.5	141.3	900	143.1	155.2	136.6
		$L_{p,pk}$	15	149.4	160.8	141.6	900	143.1	155.2	136.6
		Bottom	1146	139.4	151.5	133.2	1146	140.0	151.9	134.1
	191	L_p	50	146.4	156.8	138.9	350	134.5	143.6	129.3
		$L_{p,pk}$	50	146.4	156.8	138.9	25	132.9	144.9	128.1
		Bottom	592	137.5	149.0	132.2	592	132.2	142.5	128.9
	237	L_p	75	140.9	147.6	133.1	100	135.7	144.1	126.8
		$L_{p,pk}$	75	140.9	147.6	133.1	100	135.7	144.1	126.8
		Bottom	181	137.8	144.9	129.6	181	132.5	140.5	125.0
	354	L_p	50	148.5	159.4	140.8	25	141.7	154.6	134.7
		$L_{p,pk}$	50	148.5	159.4	140.8	25	141.7	154.6	134.7
		Bottom	2539	124.1	130.9	119.2	2539	124.6	132.1	119.7
150000	102	L_p	50	139.8	147.6	134.0	75	135.6	140.3	127.3
		$L_{p,pk}$	50	139.8	147.6	134.0	100	135.6	140.4	127.3
		Bottom	220	137.3	146.1	129.5	220	128.7	135.4	123.2
	180	L_p	50	148.3	158.9	140.2	400	137.7	149.1	132.1
		$L_{p,pk}$	25	148.1	159.1	139.5	400	137.7	149.1	132.1
		Bottom	758	139.9	150.4	134.8	758	134.9	147.0	131.4
	191	L_p	50	144.3	155.6	136.4	150	131.1	137.9	124.1
		$L_{p,pk}$	50	144.3	155.6	136.4	150	131.1	137.9	124.1
		Bottom	274	136.4	146.1	130.0	274	128.0	133.9	122.4
	237	L_p	50	138.7	145.8	129.2	75	129.2	136.0	120.2
		$L_{p,pk}$	75	138.2	146.4	128.6	75	129.2	136.0	120.2
		Bottom	109	133.7	142.3	124.8	109	125.6	132.4	117.1
	354	L_p	50	147.2	158.5	139.0	700	137.9	148.1	131.3
		$L_{p,pk}$	50	147.2	158.5	139.0	25	137.3	148.8	130.3
		Bottom	2644	124.2	131.8	118.2	2644	123.8	131.7	118.2

Appendix B. Acoustic Metrics

Underwater sound pressure amplitude is measured in decibels (dB) relative to a fixed reference pressure of p_0 = 1 µPa. Because the perceived loudness of sound, especially pulsed noise such as from seismic airguns, pile driving, and sonar, is not generally proportional to the instantaneous acoustic pressure, several sound level metrics are commonly used to evaluate noise and its effects on marine life. Here we provide specific definitions of relevant metrics used in the accompanying report. Where possible, we follow the American National Standard Institute and International Organization for Standardization definitions and symbols for sound metrics (e.g., ISO 2017, ANSI R2013), but these standards are not always consistent.

The zero-to-peak sound pressure, or peak sound pressure (PK or $L_{p,pk}$; dB re 1 µPa), is the decibel level of the maximum instantaneous acoustic pressure in a stated frequency band attained by an acoustic pressure signal, $p(t)$:

$$L_{\mathrm{p,pk}} = 10\log_{10}\frac{\max|p^2(t)|}{p_0^2} = 20\log_{10}\frac{\max|p(t)|}{p_0} \tag{B-1}$$

PK is often included as a criterion for assessing whether a sound is potentially injurious; however, because it does not account for the duration of a noise event, it is generally a poor indicator of perceived loudness.

The sound pressure level (SPL or L_p; dB re 1 µPa) is the root-mean-square (rms) pressure level in a stated frequency band over a specified time window (T; s). It is important to note that SPL always refers to an rms pressure level and therefore not instantaneous pressure:

$$L_{\mathrm{p}} = 10\log_{10}\left(\frac{1}{T}\int_T g(t)\,p^2(t)\,dt \Big/ p_0^2\right) \tag{B-2}$$

where $g(t)$ is an optional time weighting function. In many cases, the start time of the integration is marched forward in small time steps to produce a time-varying SPL function. For short acoustic events, such as sonar pulses and marine mammal vocalizations, it is important to choose an appropriate time window that matches the duration of the signal. For in-air studies, when evaluating the perceived loudness of sounds with rapid amplitude variations in time, the time weighting function $g(t)$ is often set to a decaying exponential function that emphasizes more recent pressure signals. This function mimics the leaky integration nature of mammalian hearing. For example, human-based fast time-weighted SPL ($L_{p,fast}$) applies an exponential function with time constant 125 ms. A related simpler approach used in underwater acoustics sets $g(t)$ to a boxcar (unity amplitude) function of width 125 ms; the results can be referred to as $L_{p,boxcar\ 125ms}$.

The sound exposure level (SEL or L_E; dB re 1 µPa²·s) is the time-integral of the squared acoustic pressure over a duration (T):

$$L_{\mathrm{E}} = 10\log_{10}\left(\int_T p^2(t)\,dt \Big/ T_0 p_0^2\right) \tag{B-3}$$

where T_0 is a reference time interval of 1 s. SEL continues to increase with time when non-zero pressure signals are present. It is a dose-type measurement, so the integration time applied must be carefully considered in terms of relevance for impact to the exposed recipients.

SEL can be calculated over a fixed duration, such as the time of a single event or a period with multiple acoustic events. When applied to pulsed sounds, SEL can be calculated by summing the SEL of the N individual pulses. For a fixed duration, the square pressure is integrated over the duration of interest. For multiple events, the SEL can be computed by summing (in linear units) the SEL of the N individual events:

$$L_{\mathrm{E,N}} = 10 \log_{10} \sum_{i=1}^{N} 10^{\frac{L_{E,i}}{10}} \quad \text{(B-4)}$$

Appendix C. Marine Mammal Impact Criteria

C.1. Sound Pressure Level (SPL)

The National Marine Fisheries Service (NMFS) SPL criteria for injury to marine mammals from acoustic exposure were set according to recommendations for cautionary estimates of sound levels leading to onset of permanent hearing threshold shift (PTS). These criteria prescribed injury thresholds of 190 dB re 1 µPa SPL for pinnipeds and 180 dB re 1 µPa SPL for cetaceans, for all types of sound sources except tactical sonar and explosives (NMFS 2016). These injury thresholds are applied to individual noise pulses or instantaneous sound levels and do not consider the overall duration of the noise or its acoustic frequency distribution.

Criteria that do not account for exposure duration or noise spectra are generally insufficient on their own for assessing hearing injury.

C.2. Sound Exposure Level (SEL) and Peak SPL

In recognition of shortcomings of the SPL-only based injury criteria, in 2005 NMFS sponsored the Noise Criteria Group to review literature on marine mammal hearing to propose new noise exposure criteria. Members of this expert group published a landmark paper (Southall et al. 2007) that suggested assessment methods similar to those applied for humans. The resulting recommendations introduced dual acoustic injury criteria for impulsive sounds that included peak pressure level thresholds and SEL_{24h} thresholds, where the subscripted 24 h refers to the accumulation period for calculating SEL.

SEL_{24h} is frequency weighted according to one of five marine mammal species hearing groups: low-, mid- and high-frequency cetaceans (LFC, MFC, and HFC respectively) and phocids, earless or true seals (pinnipeds), and otariids, eared seals (PPW and OPW, respectively). The onset threshold levels for Temporary Threshold Shift (TTS) and Permanent Threshold Shift (PTS) differ by group and are applied to M-weighted SEL.

C.2.1. Marine mammal auditory weighting functions (NMFS 2018)

In 2015, a U.S. Navy technical report by Finneran (2015) recommended new auditory weighting functions. The overall shape of the auditory weighting functions is similar to human A-weighting functions, which follows the sensitivity of the human ear at low sound levels. The new frequency-weighting function is expressed as:

$$G(f) = K + 10\log_{10}\left[\left(\frac{(f/f_{lo})^{2a}}{\left[1+(f/f_{lo})^{2}\right]^{a}\left[1+(f/f_{hi})^{2}\right]^{b}}\right)\right], \quad \text{(C-1)}$$

Finneran (2015) proposed five functional hearing groups for marine mammals in water: low-, mid-, and high-frequency cetaceans, phocid pinnipeds, and otariid pinnipeds. The parameters for these frequency-weighting functions were further modified the following year (Finneran 2016) and were adopted in NOAA's technical guidance that assesses noise impacts on marine mammals (NMFS 2016), which was updated two years later after extensive consultations within the scientific community (NMFS 2018). The updates did not affect the content related to either the m-weighting functions definitions or the threshold values. Table C-1 lists the frequency-weighting parameters for each hearing group; Figure C-1 shows the resulting frequency-weighting curves.

Table C-1. Parameters for the auditory weighting functions recommended by NMFS (2018).

Hearing group	*a*	*b*	f_{lo} (Hz)	f_{hi} (Hz)	*K* (dB)
Low-frequency cetaceans	1.0	2	200	19,000	0.13
Mid-frequency cetaceans	1.6	2	8,800	110,000	1.20
High-frequency cetaceans	1.8	2	12,000	140,000	1.36
Phocid pinnipeds in water	1.0	2	1,900	30,000	0.75
Otariid pinnipeds in water	2.0	2	940	25,000	0.64

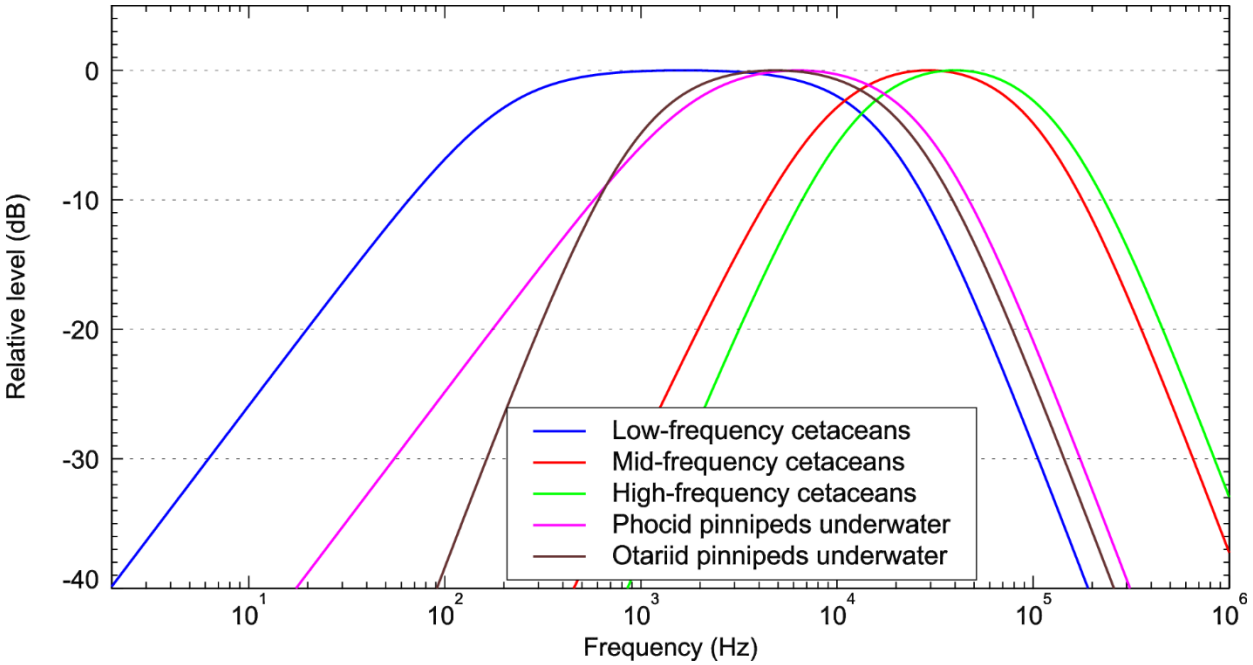

Figure C-1. Auditory weighting functions for functional marine mammal hearing groups as recommended by NMFS (2018).

C.2.2. Impact thresholds (NMFS 2018)

The PTS- and TTS-onset threshold levels for each hearing group (NMFS 2018) are listed in Table C-2. The threshold levels are defined separately for impulsive sources (e.g., seismic airgun arrays, echosounders) and non-impulsive sources (e.g., vessels). The SEL thresholds are applicable to weighted acoustic fields, while the peak SPL fields are tested against the thresholds without application of the weighting functions.

Table C-2. TTS- and PTS-onset levels for defined marine mammal groups by NMFS (2018).

Hearing group	Non-impulsive		Impulsive			
	SEL (weighted) (dB re 1 µPa²·s)		SEL (weighted) (dB re 1 µPa²·s)		peak SPL (non-weighted) (dB re 1 µPa)	
	TTS-onset	PTS-onset	TTS-onset	PTS-onset	TTS-onset	PTS-onset
Low-frequency cetaceans (LFC)	179	199	168	183	213	219
Mid-frequency cetaceans (MFC)	178	198	170	185	224	230
High-frequency cetaceans (HFC)	153	173	140	155	196	202
Phocid pinnipeds underwater (PPW)	181	201	170	185	212	218
Otariid pinnipeds in water (OPW)	199	219	188	203	226	232